

Local susceptibility and Kondo scaling in the presence of finite bandwidth

Markus Hanl and Andreas Weichselbaum

*Physics Department, Arnold Sommerfeld Center for Theoretical Physics,
and Center for NanoScience, Ludwig-Maximilians-Universität, 80333 Munich, Germany*

(Dated: February 26, 2014)

The Kondo scale T_K for impurity systems is expected to guarantee universal scaling of physical quantities. However, in practice, not every definition of T_K necessarily supports this notion away from the strict scaling limit. Specifically, this paper addresses the role of finite bandwidth D in the strongly-correlated Kondo regime. For this, various theoretical definitions of T_K are analyzed based on the inverse magnetic impurity susceptibility at zero temperature. While conventional definitions in that respect quickly fail to ensure universal Kondo scaling for a large range of D , this paper proposes an altered definition of T_K^{sc} that allows universal scaling of dynamical or thermal quantities for a given fixed Hamiltonian. If the scaling is performed with respect to an external parameter which directly enters the Hamiltonian, such as magnetic field, the corresponding $T_K^{\text{sc,B}}$ for universal scaling differs, yet becomes equivalent to T_K^{sc} in the scaling limit. The only requirement for universal scaling in the full Kondo parameter regime with a residual error of less than 1% is a well-defined isolated Kondo feature with $T_K \lesssim 0.01 D$, irrespective of specific other impurity parameter settings. By varying D over a wide range relative to the bare energies of the impurity, for example, this allows a smooth transition from the Anderson to the Kondo model.

PACS numbers: 02.70.-c, 05.10.Cc, 75.20.Hr, 72.15.Qm,

I. INTRODUCTION

The Kondo scale represents a dynamically generated low-energy scale which arises when an unpaired spin, to be referred to as the impurity, is screened by a metallic host. Prototypical examples include actual dilute magnetic impurities in metals,¹⁻⁴ but also highly controllable quantum dot settings which are characterized through transport measurements.^{5,6} The precise definition of the Kondo scale, however, is usually subject to conventions. Nevertheless, whatever the definition of the Kondo scale T_K , clean isolated Kondo features are expected to be universal: that is after proper scaling w.r.t. T_K , the resulting data is expected to fully collapse onto a single universal curve. Therefore whatever the specific definition of the Kondo scale, e.g. up to an irrelevant definition-dependent prefactor of order one, this represents an important stringent requirement: T_K must allow for accurate scaling of Kondo related features. A prototypical application that requires such scaling, for example, is the analysis of the prefactors in Fermi-liquid scaling of interacting impurity models,⁷⁻¹⁰ which strongly depends on the precise definition of T_K . As a matter of fact, the present work emerged and thus was motivated from preliminary work in exactly this direction for multi-band models,^{4,11} with the results on the related Fermi liquid coefficients to be published elsewhere.

With T_K typically described by an exponential expression,¹² the terms in the exponent usually do not depend on the full bandwidth D of a given model. The prefactor in the definition of T_K , however, may depend on D with the consequence that certain definitions of T_K can spoil universal Kondo scaling *even if* $T_K \ll D$. Consider, for example, the standard single impurity Anderson model (SIAM, see model Hamiltonian further be-

low) with the impurity onsite interaction U . For $U \ll D$ the full bandwidth D becomes irrelevant for the impurity related physics. This turns out to be the safe regime for impurity related quantities. For the case $U \gtrsim D$, however, the bandwidth D becomes relevant for Kondo related quantities. Importantly, this regime is (i) experimentally relevant, in that the experiment is never truly in the Kondo scaling limit. Moreover, through Schrieffer-Wolff transformation in the limit $U \rightarrow \infty$ of the particle-hole symmetric SIAM, (ii) this leads to the Kondo model, a widely used model itself. With its Kondo temperature given by $T_K \simeq D\sqrt{2\nu J}e^{-1/(2\nu J)}$,^{1,12,13} with J the Kondo coupling and ν the density of states at the Fermi edge, this model is *intrinsically and strongly* affected by finite bandwidth. Therefore, in particular, the present discussion is of clear relevance also for the Kondo model.

Proper Kondo scaling is already built-in by construction in the experiment-like approach of using (full-width-) half-maximum type measures of T_K ,^{5,6} which strictly focuses on the low-energy features of the measured quantities, typically assuming $T_K \ll D$. However, this requires to measure or calculate an entire curve while possibly subtracting a broader background still.⁴ In contrast, for the theoretical analysis it appears more desirable to have a single measurable quantity, instead, which uniquely defines T_K up to a convention-dependent constant prefactor of order one. To be specific, this requires a definition of T_K at zero temperature in the absence of magnetic field in a static context, i.e. $T = B = \omega = 0$ (using $k_B = g\mu_B = \hbar = 1$ throughout, for convenience). This T_K is measured through a weak perturbation of the system, and hence can be computed within linear response. Considering that the Kondo state is sensitive to an external magnetic field, the quantity of interest discussed in this paper is the magnetic susceptibility of the impurity. The following discussion, however, can be

generalized to other local susceptibilities.

A standard definition for the Kondo temperature for the one-channel Kondo model is given by^{12,14}

$$T_K \equiv \frac{1}{4\chi_0}, \quad (1)$$

with $\chi_0 \equiv \lim_{T \rightarrow 0} \chi(T)$ the static magnetic susceptibility of the impurity in the limit of zero temperature. The constant prefactor of 1/4 is part of the definition which may be chosen differently, for example, for multi-channel models.¹² The immanent question, however, that arises with Eq. (1) is, how does one precisely define the impurity contribution χ_0 to the magnetic susceptibility? The predominant conventions to be found in the literature are,^{12,14–16}

$$\chi^{(d)}(T) \equiv \langle \hat{S}_z^d \| \hat{S}_z^d \rangle_T \quad (2a)$$

$$\chi^{\text{tot}}(T) \equiv \langle \hat{S}_z^{\text{tot}} \| \hat{S}_z^{\text{tot}} \rangle_T - \langle \hat{S}_z^{\text{tot}} \| \hat{S}_z^{\text{tot}} \rangle_T^{(0)}. \quad (2b)$$

where $\langle \hat{S}^\alpha \| \hat{S}^\beta \rangle \equiv \frac{d}{dB} \langle \hat{S}^\beta \rangle \Big|_{B=0}$ describes the static linear spin susceptibility of $\langle \hat{S}^\beta \rangle$ in response to the perturbation $\hat{H}' = -B\hat{S}^\alpha$ with B an external magnetic field (the minus sign in \hat{H}' ensures $\chi \geq 0$ if $\hat{S}^\alpha = \hat{S}^\beta$). Here \hat{S}_z^d (\hat{S}_z^{tot}) stands for the total spin of the impurity (the entire system), respectively. Since, in general, the spin of the impurity \hat{S}_z^d is not conserved and hence does not commute with the Hamiltonian, Eq. (2a) is equivalent to the evaluation of a dynamical correlation function.¹⁴ It is a somewhat abstract quantity since from an experimental point of view it is difficult to just apply a magnetic field at the impurity itself. The second definition of the impurity susceptibility in Eq. (2b), on the other hand, is typically considered closer to an experimental realization, in that the impurity contribution to the total susceptibility is evaluated by taking the difference of the total susceptibility with $[\langle \cdot \rangle_T]$ and without $[\langle \cdot \rangle_T^{(0)}]$ the impurity, where the latter acts as a reference system. Eq. (2b) includes the total spin \hat{S}_z^{tot} of the system, which is assumed to be conserved and hence is simply proportional to the overall spin fluctuations, $\langle \hat{S}_z^{\text{tot}} \| \hat{S}_z^{\text{tot}} \rangle_T = \beta(\langle (\hat{S}_z^{\text{tot}})^2 \rangle - \langle \hat{S}_z^{\text{tot}} \rangle^2)$ where $\beta \equiv 1/T$. Hence, in principle, it is easier to evaluate. However, from a computational point of view it has the disadvantage that one essentially needs two calculations, one with and one without the impurity, followed by the subtraction of two extensive macroscopic and thus large values in order to obtain an intrinsic impurity-related finite quantity. While one may expect that both definitions in Eqs. (2) give comparable results, they are not strictly equivalent. In particular, neither definition in Eqs. (2) necessarily guarantees proper scaling of Kondo related features at finite bandwidth.

Scaling onto a universal curve requires an appropriate and consistent set of parameters. For the Kondo physics analyzed in this paper, these are simply a particle-hole symmetric setting (or a similarly consistent asymmetric setting, e.g. $U/\varepsilon_d = \text{const}$ for the SIAM below), together with the bare requirement of a well-defined isolated low-energy feature with $T_K \lesssim 0.01 D$, e.g. the

Kondo peak in the spectral function, which allows to observe Kondo physics to start with. Here universal scaling is understood in the usual way. Given a set of individual curves $y(x; \{p\})$, when plotted vs. x , these depend on a set $\{p\}$ of external model parameters. Here x represents an energy, e.g. $x \in \{\omega, T, B, \dots\}$. Therefore universal scaling of x by an appropriately chosen Kondo scale $T_K^{\text{sc},x}$, i.e. $\tilde{x} \equiv x/T_K^{\text{sc},x}$, implies that the curves $y(T_K^{\text{sc},x}\tilde{x}; \{p\})/y_0 =: \tilde{y}(\tilde{x})$ collapse onto a single universal curve $\tilde{y}(\tilde{x})$ independent of $\{p\}$. Note, that away from the Kondo scaling limit, this Kondo scale $T_K^{\text{sc},x}$ can depend on the specific $x \in \{\omega, T, B, \dots\}$ chosen. Moreover, the vertical normalization y_0 of the curves is not necessarily related to $T_K^{\text{sc},x}$. Rather, it depends on the measured quantity which may not even have units of energy. Typically, the specific choice for y_0 emerges out of context in a straightforward way, and as such is specified with each application below.

The main result of this paper is the proposition of the altered definition of the impurity susceptibility,

$$\chi^{\text{sc}}(T) \equiv \langle \hat{S}_z^{\text{tot}} \| \hat{S}_z^{\text{tot}} \rangle_T - \langle \hat{S}_z^{\text{bath}} \| \hat{S}_z^{\text{bath}} \rangle_T \quad (3a)$$

$$= 2\langle \hat{S}_z^d \| \hat{S}_z^{\text{tot}} \rangle_T - \langle \hat{S}_z^d \| \hat{S}_z^d \rangle_T, \quad (3b)$$

used for the scaling of dynamical or thermal quantities, i.e. $x \in \{\omega, T\}$. Here $\hat{S}_z^{\text{bath}} \equiv \hat{S}_z^{\text{tot}} - \hat{S}_z^d$ and $\langle \hat{S}^\alpha \| \hat{S}^\beta \rangle$ as defined with Eq. (2). As will be demonstrated numerically, the definition of the susceptibility in Eq. (3) provides a sensitive Kondo scale through Eq. (1), i.e. $T_K^{\text{sc}} \equiv \lim_{T \rightarrow 0} 1/(4\chi^{\text{sc}}(T)) \equiv 1/(4\chi_0^{\text{sc}})$, which allows for proper scaling (sc) of frequency or temperature dependent curves onto a single universal curve in a wide range of impurity parameters with bare energies from much smaller to much larger than the bandwidth D , provided that one has a well-defined Kondo regime, i.e. $T_K \ll D$. For notational simplicity, x will not be specified with T_K here, i.e. $T_K^{\text{sc}} \equiv T_K^{\text{sc},\omega} \equiv T_K^{\text{sc},T}$. A motivation of Eq. (3) in terms of the non-interacting system is given in the App. A. More generally, as pointed out with App. A 2, above scale-preserving susceptibility may be understood in terms of the scaling of frequency by the quasi-particle weight z .¹⁷

In contrast, the earlier definitions in Eqs. (2) can be reliably used for scaling in certain parameter regimes only (e.g. the scaling limit when the bandwidth is the largest energy scale by far). The major differences of the impurity susceptibility in Eq. (3) to the definitions in Eqs. (2) are apparent. As compared to Eq. (2b), the last term in Eq. (3a) is calculated *in the presence* of the impurity. This comes with the benefit that, similar to Eq. (2a), Eq. (3b) can be computed entirely through the *non-extensive* quantities since the extensive leading term in Eq. (3a) cancels. Therefore, in contrast to Eq. (2b), the impurity susceptibility in Eq. (3) can be computed for a given system without having to resort to a reference system without the impurity. Compared to Eq. (2a), on the other hand, Eq. (3) acquires the relevant correction $\langle \hat{S}_z^d \| \hat{S}_z^d \rangle_T \rightarrow \langle \hat{S}_z^d \| \hat{S}_z^d \rangle_T - 2[\langle \hat{S}_z^d \| \hat{S}_z^d \rangle_T - \langle \hat{S}_z^d \| \hat{S}_z^{\text{tot}} \rangle_T]$.

dependence on	universal Kondo scale $T_K = \frac{1}{4\chi_0^d}$	correction to χ_0^d	see also
ω or T	T_K^{sc} where $\chi_0^{\text{sc}} = 2\chi_0^{\text{FS}} - \chi_0^d$	$2 \times (\chi_0^{\text{FS}} - \chi_0^d)$	Eq. (3)
B	$T_K^{\text{sc},B}$ where $\chi_0^{\text{sc},B} = \chi_0^{\text{FS}}$	$1 \times (\chi_0^{\text{FS}} - \chi_0^d)$	Eq. (4)

Table I. Proposed corrections to the Kondo temperature based on the commonly used zero-temperature impurity susceptibility χ_0^d away from the strict scaling limit of infinite bandwidth, yet in the Kondo regime having $T_K \lesssim 10^{-2}D$. In the scaling limit, all corrections vanish, i.e. $\chi_0^{\text{FS}} = \chi_0^d$.

For the T_K^{sc} derived from Eq. (3), the emphasis is on a given fixed Hamiltonian with infinitesimal perturbations whose (many-body) excitations are explored either dynamically or thermally. For this, the Kondo scale derived from χ_0^{sc} mimics the scaling limit, even if the parameters that enter the Hamiltonian do not strictly adhere to the scaling limit. In contrast, as will be shown below, *if the Hamiltonian itself* is altered through an external parameter $x \in \{B, \dots\}$ via $\hat{H}' = -x\hat{X}$, universal scaling vs. a finite range in x analyzed at zero temperature is generally governed by a slightly different Kondo scale, $T_K^{\text{sc},x}$, based on a variant of the impurity susceptibility (henceforth, the notation $T_K^{\text{sc},x}$ will be reserved for this context only).

In the scaling limit where bandwidth is the largest energy scale by far, it is found that $\langle \hat{S}_z^d \| \hat{S}_z^{\text{tot}} \rangle_T \simeq \langle \hat{S}_z^d \| \hat{S}_z^d \rangle_T$ (for a proof of this in the non-interacting case, see App. A 2). Only in this regime, the static magnetic susceptibility can be computed equivalently in various ways including Eqs. (2), i.e. $\chi^{\text{sc}}(T) \simeq \chi^d(T) \simeq \chi^{\text{FS}}(T)$. Here, in particular, the more conventional magnetic susceptibility $\chi^d(T)$ may be replaced by $\chi^{\text{FS}}(T)$ which is much simpler and cheaper to evaluate.

The definitions for proper scale-preserving Kondo temperatures at finite bandwidth as proposed in this paper are summarized in Tbl. I. This includes the Kondo temperature T_K^{sc} for fixed Hamiltonian for scaling of dynamical or thermal quantities, as well as the Kondo temperature $T_K^{\text{sc},B}$ for scaling vs. an external parameter that alter the Hamiltonian at $T = \omega = 0$, here for the specific case of magnetic field B . The derivation of the latter (see Sec. II C) may also serve as a general guide for scaling vs. other external physical parameters that directly enter the Hamiltonian.

The remainder of the paper then is organized as follows: The rest of the introduction discusses the role of the new susceptibility $\langle \hat{S}_z^d \| \hat{S}_z^{\text{tot}} \rangle_T$ introduced with Eq. (3) in terms of the Friedel sum rule (Sec. IA). Furthermore, Sec. I still provides general computational aspects on the static linear susceptibility (Sec. IB), followed by model conventions and methods (Sec. IC). Sec. II presents the results and discussion on the scaling of dynamical impurity spin susceptibility (vs. frequency), as well as the scaling of the linear conductance (vs. temperature and magnetic field). Following summary and outlook, the appendices provides detailed technical discussions. It includes (App. A) a motivation for the scale-preserving susceptibility which is mainly based on the non-interacting system, (App. B) a technical discussion of finite-size effects

of the dynamical impurity susceptibility, and (App. C) technicalities on the evaluation of the mixed susceptibility $\chi^{\text{FS}}(T)$ within the fdm-NRG framework. The latter also contains a short discussion on the evaluation of the impurity specific heat which, in a wider sense, also resembles the structure of an impurity susceptibility. Finally, App. D comments on the conventional extraction of phase shifts from the many-body fixed-point spectra of the NRG, while also providing a detailed analysis of discretization, i.e. finite size, effects.

A. Magnetic susceptibility and Friedel sum rule

The definition of the impurity susceptibility in Eq. (3) introduces the additional impurity susceptibility,

$$\chi^{\text{FS}}(T) \equiv \langle \hat{S}_z^d \| \hat{S}_z^{\text{tot}} \rangle_T = \beta \langle \hat{S}_z^{\text{tot}} \hat{S}_z^d \rangle_T, \quad (4)$$

where $\beta \equiv 1/T$, and ‘FS’ stands for Friedel sum rule as motivated shortly. It will also be referred to as *mixed* susceptibility, as it combines the impurity spin with the total spin. Assuming $B = 0$, the last equality in Eq. (4) used $\langle \hat{S}_z^{\text{tot}} \rangle_T = \langle \hat{S}_z^d \rangle_T = 0$. Given that \hat{S}_z^{tot} commutes with the Hamiltonian, this reduces to the simple thermal expectation value as indicated, which can be evaluated efficiently (see App. C for details). Consequently, for $T = 0^+$, this corresponds to a *strict* low-energy quantity that does not further explore the dynamics at intermediate or large frequency $\omega > T_K$ [which is the case, for example, for the definition of the impurity susceptibility in Eq. (2a)].

The susceptibility in Eq. (4) can be interpreted twofold: (i) as the local contribution to the total magnetization due to a global external field, or equivalently, (ii) as the response in the total magnetization of the system due to a local magnetic field at the impurity only. The first can be seen as (yet another) intuitive and qualitative description of the local spin susceptibility. The latter interpretation, on the other hand, allows a direct link to the Friedel-sum-rule (FS) [hence the label in Eq. (4)]: given an (infinitesimal) local change of the Hamiltonian. FS relates the low-energy phase shifts φ_σ of the entire system to the *total* change in local charge that flows to or from infinity (note that this change in local charge includes the displaced charge of both, the impurity itself as well as the close vicinity of the impurity, which in total may simply be interpreted as displaced ‘local’ charge¹⁸).

The dependence of the low-energy phase shifts φ_σ of the bath electrons on an external magnetic field at the

impurity can be used to define a Kondo scale T_K^φ ,⁷

$$\lim_{B \rightarrow 0} \frac{d}{dB} \varphi_\sigma \equiv \sigma \frac{\pi}{4T_K^\varphi}, \quad (5)$$

evaluated at $T = 0$, where $\sigma \in \{\uparrow, \downarrow\} \equiv \pm 1$. As a direct consequence of the Friedel-sum-rule then, it follows

$$T_K^\varphi = T_K^{\text{FS}}, \quad (T = 0) \quad (6)$$

since $\langle \hat{S}_z^{\text{tot}} \rangle = \frac{1}{2}(\Delta N_\uparrow - \Delta N_\downarrow) \stackrel{\text{FS}}{=} \frac{1}{2\pi}(\varphi_\uparrow - \varphi_\downarrow)$, with ΔN_σ the change in total number of particles with spin σ relative to $B = 0$. Consequently, $\chi^{\text{FS}} \equiv \frac{d}{dB_{\text{imp}}} \langle \hat{S}_z^{\text{tot}} \rangle = 1/(4T_K^\varphi)$, which coincides with the definition of T_K^{FS} , and hence proves Eq. (6). The identity in Eq. (6) has also been verified numerically to within 1% accuracy (using NRG with $\Lambda = 2$ as defined below; for a more detailed discussion on the explicit extraction of phase shifts within the NRG, see App. D).

While, intuitively, one may have expected that the dependence of the low-energy phase shifts on the magnetic field yields a universal Kondo scale, this is true only in the specific case that data is scaled vs. magnetic field at $T = \omega = 0$, i.e. having $x = B$ (see Sec. II C further below). However, this alters the Hamiltonian. For dynamical or thermal quantities for a given fixed Hamiltonian, having Eq. (3b), T_K^{FS} does not guarantee universal scaling. The reason for this may be seen as follows: while, in fact, the phase shifts themselves are not necessarily affected by finite bandwidth at $B = 0^+$, i.e. at the low-energy fixed point [cf. the discussion of χ_0^{FS} for the non-interacting case in App. A 2], when investigating an entire universal curve w.r.t. to frequency or temperature, this necessarily also explores states at intermediate energies. By exploring a range of energies, however, this becomes susceptible to finite bandwidth. Hence T_K^φ fails to provide proper scaling onto a universal curve for dynamical or thermal data.

B. Static linear susceptibility

Consider the general static linear susceptibility for obtaining a response in the measured operator $\langle \hat{Y} \rangle$ by applying the infinitesimal external perturbation $\hat{H}'(\lambda) = -\lambda \hat{X}$ to a given Hamiltonian,

$$\langle \hat{X} \| \hat{Y} \rangle_T \equiv \lim_{\lambda \rightarrow 0} \frac{d}{d\lambda} \langle \hat{Y} \rangle_{T, \lambda} = \int_0^\beta d\tau \langle \delta \hat{X}(\tau) \cdot \delta \hat{Y} \rangle_T, \quad (7)$$

with $\beta \equiv 1/T$, $\delta \hat{X} \equiv \hat{X} - \langle \hat{X} \rangle_T$, similarly for $\delta \hat{Y}$, and $\hat{X}(\tau) \equiv e^{\tau \hat{H}} \hat{X} e^{-\tau \hat{H}}$ evaluated at $\lambda = 0$. By definition, the operators \hat{X} and \hat{Y} are assumed hermitian. The last equality in Eq. (7), i.e. the imaginary-time Matsubara susceptibility, represents an *exact* mathematical relation,¹⁹ which satisfies the properties of a scalar product for hermitian operators, i.e. $\langle \hat{X} \| \hat{Y} \rangle_T \equiv \langle \hat{Y} \| \hat{X} \rangle_T^*$ with

$\langle \hat{X} \| \hat{X} \rangle_T \geq 0$ (cf. Bogoliubov-Kubo-Mori scalar product [19]). If \hat{X} and \hat{Y} do not commute with the Hamiltonian and $\langle \hat{X} \rangle_T = \langle \hat{Y} \rangle_T = 0$, then Eq. (7) is equivalent to the Kubo formula for linear response in the thermodynamic limit,

$$\langle \hat{X} \| \hat{Y} \rangle_T \simeq \langle \hat{X} \| \hat{Y} \rangle_T^{(R)} \equiv - \lim_{\omega \rightarrow 0} \chi_{\hat{X}\hat{Y}}^R(\omega) \quad (8)$$

with $\chi_{\hat{X}\hat{Y}}^R(\omega)$ the Fourier transformed dynamical retarded (R) correlation function $\chi_{\hat{X}\hat{Y}}^R(t) \equiv -i\vartheta(t) \langle [\hat{X}(t), \hat{Y}] \rangle_T$ [the sign with the last term in Eq. (8) originates in the sign of the definition of \hat{H}' with Eq. (7) which ensures a positive susceptibility for $\hat{X} = \hat{Y}$]. The Kubo formula as in Eq. (8), however, assumes that the system has no long-time memory of the applied operators \hat{X} or \hat{Y} . Importantly, for exactly this reason for discretized, i.e. effectively finite-size systems, only Eq. (7) represents a reliable working definition, whereas corrections can apply to Eq. (8) [e.g. see App. B]. Most notably, if the Hamiltonian preserves total spin (which will be assumed throughout this paper), then with $\hat{X} = \hat{Y} = \hat{S}_z^{\text{tot}}$, the resulting dynamical correlation function $\text{Im} \chi(\omega) \propto 0 \cdot \delta(\omega)$ is pathological. In contrast, Eq. (7) yields the correct result $\langle \hat{S}_z^{\text{tot}} \| \hat{S}_z^{\text{tot}} \rangle_T = \beta \langle (\hat{S}_z^{\text{tot}})^2 \rangle_T - \langle \hat{S}_z^{\text{tot}} \rangle_T^2 \equiv \beta \Delta^2 S_z^{\text{tot}}$, i.e. the thermal fluctuations in the total spin of the system, using the grand-canonical ensemble in the evaluation of the thermal average $\langle \cdot \rangle_T$.

C. Models and method

A prototypical quantum impurity model is the single impurity Anderson model (SIAM).^{20,21} It consists of the local Hamiltonian, $\hat{H}_0^{\text{SIAM}} \equiv \hat{H}_{\text{imp}} + \hat{H}_{\text{cpl}}$, with

$$\hat{H}_{\text{imp}} = \sum_\sigma \varepsilon_{d\sigma} \hat{n}_{d\sigma} + U \hat{n}_{d\uparrow} \hat{n}_{d\downarrow} \quad (9a)$$

$$\hat{H}_{\text{cpl}} = \sum_{k\sigma} (V_{k\sigma} \hat{d}_\sigma^\dagger \hat{c}_{k\sigma} + \text{H.c.}) \equiv \sqrt{\frac{2D\Gamma}{\pi}} \sum_\sigma (\hat{d}_\sigma^\dagger \hat{f}_{0\sigma} + \text{H.c.}). \quad (9b)$$

It describes a single interacting fermionic (d-)level, i.e. the impurity (imp), with level-position $\varepsilon_{d\sigma}$ and onsite interaction U , which is coupled (cpl) through hybridization to a non-interacting macroscopic Fermi sea $\hat{H}_{\text{bath}} \equiv \sum_{k\sigma} \hat{n}_{k\sigma}$ with $\varepsilon_{k\sigma} \in [-D, D]$ of half-bandwidth $D := 1$ (all energies taken in units of D , unless specified otherwise). Here \hat{d}_σ^\dagger ($\hat{c}_{k\sigma}^\dagger$) creates an electron with spin $\sigma \in \{\uparrow, \downarrow\}$ at the d-level (in the bath at momentum k), respectively, with $\hat{n}_{d\sigma} \equiv \hat{d}_\sigma^\dagger \hat{d}_\sigma$, and $\hat{n}_{k\sigma} \equiv \hat{c}_{k\sigma}^\dagger \hat{c}_{k\sigma}$. If a magnetic field is applied at the impurity (in the bath), then $\varepsilon_{d\sigma} = \varepsilon_d - \frac{\sigma}{2}B$ ($\varepsilon_{k\sigma} = \varepsilon_k - \frac{\sigma}{2}B$), respectively. The sign has been chosen such, that for $B > 0$ a positive magnetization $\langle \hat{S}_z \rangle$ arises. With ν the density of states, $\Gamma_\sigma(\varepsilon) \equiv \pi \nu V_\sigma^2(\varepsilon) = \Gamma \cdot \theta(D - |\omega|)$ is the hybridization strength. It is taken constant and the same for each spin σ , for simplicity.

In the limit of large U , the SIAM reduces to the Kondo model with a singly occupied impurity (a fluctuating spin), which couples to the electrons in the bath through the spin-spin interaction^{1,12}

$$\hat{H}_0^{\text{Kondo}} = 2J \hat{\mathbf{S}}_d \cdot \hat{\mathbf{S}}_0 \quad (10)$$

with $J > 0$ the antiferromagnetic Heisenberg coupling (using constant density of states $\nu = 1/2D$ of the bath, for simplicity),¹² $\hat{\mathbf{S}}_d$ the spin operator of the impurity and $\hat{\mathbf{S}}_0^x \equiv \frac{1}{2} \sum_{\sigma\sigma'} \hat{f}_{0\sigma}^\dagger \tau_{\sigma\sigma'}^x \hat{f}_{0\sigma'}$, the normalized spin operator of the bath site $\hat{f}_{0\sigma}$ at the location of the impurity with τ^x the Pauli spin matrices ($x \rightarrow \{x, y, z\}$).

The generic interacting impurity setting above involves the solution of a strongly-correlated quantum many-body system, which can be simulated efficiently using the quasi-exact numerical renormalization group (NRG).^{14,22} In order to deal with arbitrary temperatures in an accurate manner, the fdm-NRG is employed^{23–25} which is based on complete basis sets.²⁶ While not explained in detail here (for this see Refs. [14, 22, and 25]), the essential NRG related computational parameters indicated with the figures below are the dimensionless logarithmic discretization parameter $\Lambda \gtrsim 2$, the truncation energy E_{tr} in rescaled units (as defined in [25]), the number N_z of z -shifts for z -averaging,²⁷ and the log-Gaussian broadening parameter σ for smooth spectral data.

II. RESULTS AND DISCUSSION

A. Scaling of dynamical susceptibility

The dynamical magnetic susceptibility of the impurity is analyzed in Fig. 1 for both the SIAM (upper panels) as well as the Kondo model (lower panels) for a wide range of parameters, resulting in a dense set of curves. For the left panels, the horizontal frequency axis is scaled by $T_K^{\text{d}} \equiv 1/(4\chi_0^{\text{d}})$, which clearly fails to reproduce a single universal curve. The universal scaling is provided only by the scaling of frequency using the altered T_K^{sc} (right panels). The residual tiny deviations stem from the data with largest T_K , i.e. with $T_K \gtrsim 10^{-3}D$.

By analyzing the universal scaling at an accuracy of $\lesssim 1\%$, this required at the very minimum a parameter setting in the strongly correlated Kondo regime. Hence the Kondo temperature was kept clearly smaller than the bandwidth, i.e. $T_K < 10^{-2}$. For the SIAM, this allowed a wide range for the interaction strength from significantly smaller to significantly larger than the bandwidth,²⁸ nevertheless, while keeping $\Gamma/U = \frac{1}{15}$ and $\varepsilon_d/U = -\frac{1}{2}$ constant [cf. Fig. 1(a); similarly, the scaling was also tested away from the particle-hole symmetric point at $\varepsilon_d/U = -\frac{1}{3}$, resulting in equally excellent scaling of the data (not shown). The scaling also was tested for the non-interacting case ($U = \varepsilon_d = 0$ yet finite Γ ; not shown) where Γ takes the role of T_K . As a consequence, in complete analogy to above, for $\Gamma < 10^{-2}$ this allowed for

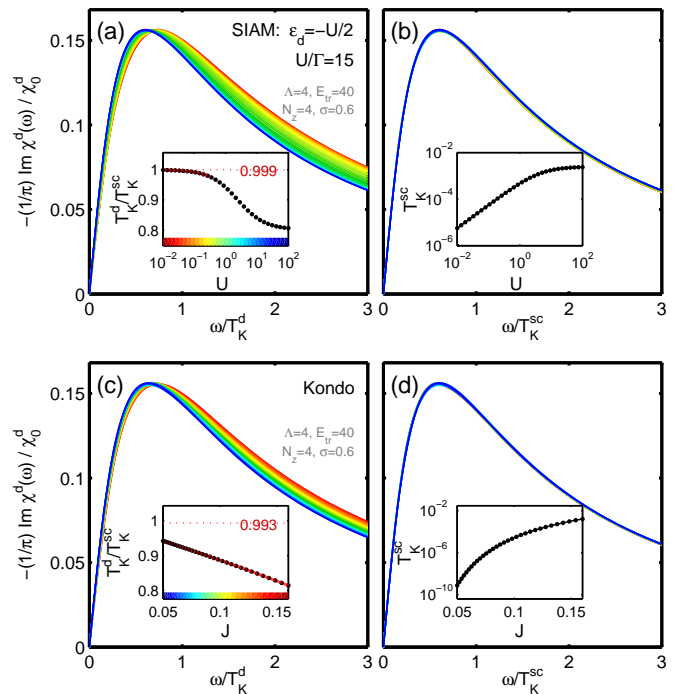


Figure 1. (Color online) Scaling of the frequency of the dynamical spin susceptibility $\chi^{\text{d}}(\omega)/\chi_0^{\text{d}}$ by the conventional impurity susceptibility $T_K^{\text{d}} \equiv 1/(4\chi_0^{\text{d}})$ (left panels) vs. the scale-preserving definition of Kondo temperature $T_K^{\text{sc}} \equiv 1/(4\chi_0^{\text{sc}})$ (right panels): all the densely lying curves of the left panels collapse onto a single universal curve in the right panels, respectively. The upper panels (a and b) analyze the SIAM. The inset to panel (a) demonstrates the dependence of $T_K^{\text{d}}/T_K^{\text{sc}}$ vs. the onsite interaction U , while keeping the ratios $U/\Gamma = 15$ and $\varepsilon_d = -U/2$ fixed. The color bar at the bottom of the lines in the main panel to the specific values of U ranging from $U \ll 1$ to $U \gg 1$ (with $D \equiv 1$ the bandwidth). The limit $\lim_{U \rightarrow 0} [T_K^{\text{d}}/T_K^{\text{sc}}]$ has been fitted, resulting in the value of 1. with excellent accuracy (actual value indicated together with the horizontal dotted line). The inset to panel (b), shows the dependence of T_K^{sc} vs. U which stretches over several orders of magnitude. In complete analogy, the lower panels (c and d) analyze the Kondo model. In particular, the fitted limit $\lim_{J \rightarrow 0} T_K^{\text{d}}/T_K^{\text{sc}} \simeq 1$ in the inset of panel (c) is the same as for the SIAM (cf. panel a) within the numerical error of significantly less than 1% [for comparison, the same calculation yet with the cheaper and less accurate setting of $\Lambda = 2$ and $E_{\text{tr}} = 12$ (not shown) already resulted in $T_K^{\text{d}}/T_K^{\text{sc}} \simeq 0.98$, while $\Lambda = 4$ and $E_{\text{tr}} = 20$ (not shown) already agreed well with above results. In this sense, above results for $\Lambda = 4$ and $E_{\text{tr}} = 40$ are considered fully converged].

similar excellent scaling of the data, yet, of course, to a different universal curve].

The different definitions of the Kondo temperature, T_K^{d} vs. T_K^{sc} , are analyzed in the insets of the left panels, showing clear deviations of T_K^{sc} from T_K^{d} of up to 20%, with T_K^{d} consistently smaller than T_K^{sc} . The deviations are more pronounced for the Kondo model, remember-

ing that this essentially reflects the large- U limit of the Anderson model, which implies $U \gg D$ (even for Kondo temperatures as small as $T_K \simeq 10^{-10}$, the difference between T_K^d and T_K^{sc} is still about 6% [see inset in lower panels]). In the limit $T_K \rightarrow 0$ both, the SIAM ($U \rightarrow 0$ with appropriately adjusted Γ and ε_d) as well as the Kondo model ($J \rightarrow 0$) result in the same ratio $T_K^d/T_K^{sc} = 1$ within the accuracy of the fitted extrapolations in the insets (using 3rd order polynomials with the fitting range indicated with the fit in red on top of the data; see caption on the convergence of T_K^d/T_K^{sc} with varying NRG parameters).

B. Scaling of static susceptibility and linear conductance vs. temperature ($B = 0$)

The scaling of the static magnetic susceptibility and the linear conductance of the SIAM and Kondo model vs. temperature is analyzed in Fig. 2. The left panels analyze the SIAM in a wide range of the onsite interaction U . The center panels analyze the SIAM still, yet in the large- U limit while varying Γ , thus transitioning to the Kondo model. The right panels, finally, analyze the Kondo model itself. In all cases the parameters were chosen such that $T_K \lesssim 10^{-2}$ with T_K plotted in the insets with the lower panels (the T_K for the largest Γ in the center panels exceeded 10^{-2} hence was excluded from the scaling analysis as indicated by the gray cross in the insets for the center panels).

The quantity $T \cdot \chi(T)$ as plotted in the upper panels of Fig. 2 for the spin susceptibility, reflects spin-fluctuations at the impurity. The high-temperature limit for the Anderson (Kondo) impurity is given by $1/8$ ($1/4$), respectively, indicated by the horizontal dashed lines. Clearly, once T exceeds U for the SIAM (or D for the Kondo model), the large temperature limit is rapidly and accurately approached for either definition of the impurity susceptibility. For the SIAM, for $U \gg D$ an intermediate regime $D < T < U$ emerges which represents a free spin, consistent with $T \cdot \chi(T) \rightarrow \frac{1}{4}$ [Fig. 2(a-b)]. For the Kondo model [Fig. 2(c)], this regime is represented by $T > D$.

In the regime $U \ll D$ for the SIAM, the effective bandwidth relevant for the impurity is given by U , such that the actual full bandwidth D of the Fermi sea becomes irrelevant in the description of the impurity [see $U = 10^{-2}$ data (dark blue) in Fig. 2(a)]. As a consequence, here the impurity susceptibility is rather insensitive to its precise definition, i.e. $\chi^d(T) \simeq \chi^{FS}(T) \simeq \chi^{sc}(T)$ [see $U = 10^{-2}$ data in inset to Fig. 2(a)], which thus is considered a safe regime for local susceptibility calculations and subsequent Kondo scaling. The differences between the three definitions of the impurity susceptibility, however, become strongly visible as U increases and surpasses the bandwidth [e.g. see $U = 10^2$ data (red curves) in Fig. 2(a)]. This behavior is precisely also reflected in the zero-temperature ratios T_K^d/T_K^{sc} as shown in the inset to Fig. 2(a), which strongly deviate from ≈ 1 as U increases.

For fixed large $U \gg D$, T_K can be strongly varied by tuning the hybridization Γ . The resulting data for the magnetic susceptibility is shown in Fig. 2(b). By plotting temperature in units of T_K^{sc} , the data for $\chi^{sc}(T)$ nicely collapses onto a universal curve for $T < D$, a feat which, in particular, cannot be achieved for $\chi^d(T)$ in a similarly accurate manner. Furthermore, having $U \gg D$, the data in Fig. 2(b) for $T < U$ clearly resembles the Kondo model, as can be seen by direct comparison to the data of the actual Kondo model in Fig. 2(c).

The lower panels of Fig. 2 analyze the scaling of the linear conductance as measured in transport through a quantum dot which represents a prototypical *quantum impurity* setting.^{5,6} It is computed by folding the impurity spectral function $A_\sigma(\omega; T) \equiv \int \frac{dt}{2\pi} \langle \{ \hat{d}_\sigma(t), \hat{d}_\sigma^\dagger \} \rangle_T$ with the derivative of the Fermi distribution function, i.e. $g(T) = \frac{\pi\Gamma}{2} \sum_\sigma \int d\omega A_\sigma(\omega; T) (-\frac{df}{d\omega})$ in units of $2e^2/h$. When scaling the temperature by T_K^d , the resulting data is plotted in light dashed lines, which show a clear non-universal spread akin to the earlier analysis in Fig. 1(a). In particular, the temperature $T_{1/2}^d$ where $g(T)$ passes through $1/2$ changes from 1.25 down to 1.03 in units of T_K^d , with the large- U regime for the SIAM [Fig. 2(e)] and in particular also the Kondo model itself [Fig. 2(f)] most strongly affected. In contrast, when scaling the temperature by T_K^{sc} , again an excellent scaling collapse is observed (solid lines in lower panels of Fig. 2). Note, furthermore, that the resulting $T_{1/2}^{sc} \equiv T_{1/2}/T_K^{sc} = 1.032 \pm 0.005$ nicely agrees across all panels from the SIAM [Fig. 2(a-b)] to the Kondo model [Fig. 2(c)], despite the broad parameter range analyzed. Given $\Lambda = 4$ together with $E_{tr} = 40$, these results are considered well converged [see figure caption on the convergence of $T_{1/2}/T_K^{sc}$ with NRG parameters]. Finally, note that the value for $T_{1/2}/T_K^{sc}$ above also agrees well with the one cited by Merker et al.¹⁰ which in the wide-band limit suggests $T_{1/2}/T_K^{sc} \simeq 1.04$. Overall, with $T_{1/2}/T_K^{sc}$ being constant, this is fully consistent with the fact that $T_{1/2}$ itself may serve and is frequently used as a universal definition of T_K , with a minor constant proportionality factor of 1.03 to the T_K^{sc} used here.

Above results have direct implications on the Fermi liquid coefficients derived from the conductance $g(T)$. For example, with the Fermi liquid coefficient c_T defined by $g(T) \simeq 1 - c_T(T/T_K)^2$ for $T \ll T_K$,⁷⁻¹⁰ this strongly depends on the precise definition of T_K . Note that even though T_K is apparently well-defined through the magnetic susceptibility, depending on the precise definition of the latter, nevertheless variations of up to 10% are seen in the ratio T_K^d/T_K^{sc} within a well-defined Kondo regime [cf. insets to upper panels of Fig. 2]. Therefore when using T_K^d , this systematically underestimates c_T by up to 20%. It follows from the present analysis that the correct choice for T_K in the definition of c_T is T_K^{sc} , as it reflects the scaling limit, despite using parameters that do not strictly represent the scaling limit itself. Note, however, that the strict scaling limit is given by the regime $T_K^d/T_K^{sc} \simeq 1$, which for the Kondo model through the

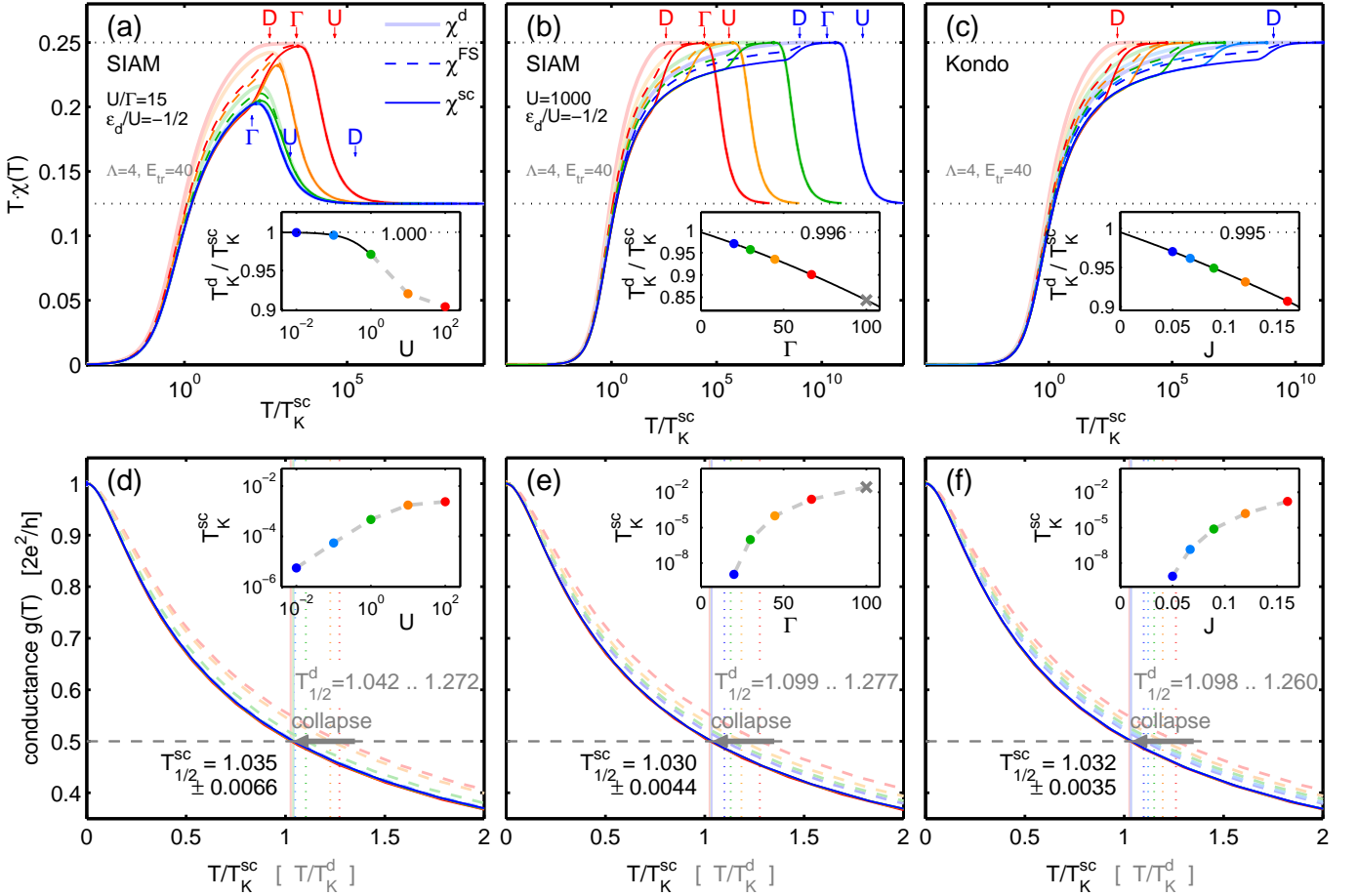


Figure 2. (Color online) Temperature dependent scaling of the static spin susceptibility $\chi(T)$ (upper panels) and the linear conductance $g(T)$ (in units of $2e^2/h$; lower panels) for the SIAM (left and center panels), as well as for the Kondo model (right panels). The color of the lines in the main panels matches the colors of the symbols in the inset, hence this indicates the respective parameter setting. The upper panels compare various definitions of the static spin susceptibility (χ^d , χ^{FS} , χ^{sc} in faint, dashed and solid, respectively). In the upper main panels, for clarity, the actual value of the relevant parameters [$\{D, \Gamma, U\}$ for panels (a-b) and D for panel (c)] are indicated in units of T_K^{sc} for the largest and smallest T_K only. Similar to Fig. 1, the insets to the upper panels analyze the relation between T_K^d and T_K^{sc} as function of the parameters. Their ratio is fitted towards $T_K \rightarrow 0$, resulting in a comparable value of 1 to very good accuracy as indicated for all three cases (panel a-c). The actual exponential range of T_K is shown in the insets to the lower panels. The lower panels show the static linear conductance $g(T)$ vs. T/T_K^d (non-universal; dashed faint lines, but color match with symbols of inset otherwise) and vs. T/T_K^{sc} (solid lines) which show proper scaling behavior, in that all lines collapse onto a single universal curve. With $T_{1/2}$ the temperature where $g(T)$ passes through 1/2, in units of T_K^d , this ranges from $T_{1/2}^d \equiv T_{1/2}/T_K^d = 1.25$ down to 1.03 [indicated by the vertical dotted lines with the range of $T_{1/2}^d$ specified with each panel (gray text at center right in each panel)]. In units of T_K^{sc} , this range collapses to the fixed value of $T_{1/2}^{sc} \equiv T_{1/2}/T_K^{sc} \simeq 1.03$ to within residual relative variations of clearly less than 1% for all three cases [panels d-f; indicated by vertical solid light lines with their range specified by $T_{1/2}^{sc}$ (black text)]. Using $\Lambda = 4$ and $E_{tr} = 40$ as indicated, the value of $T_{1/2}^{sc} \simeq 1.03$ above is considered well converged [for comparison, for $\Lambda = 2$ and $E_{tr} = 8$ a similar calculation (not shown) resulted in $T_{1/2}^{sc} \simeq 0.99$, while $\Lambda = 2$ and $E_{tr} = 12$ resulted in $T_{1/2}^{sc} \simeq 1.01$; while good overall scaling can already be observed for $E_{tr} \lesssim 10$, the minor variations for smaller E_{tr} can be mostly eliminated by normalizing $g(T)$ by the numerical value $g(0) \approx 1$ which was not included here].

inset to Fig. 2(c) implies $J \lesssim 0.01$, resulting in the extremely small and rather impractical $T_K \lesssim 10^{-45}$.

C. Scaling of linear conductance vs. magnetic field ($T = 0$)

The linear conductance at finite magnetic field yet zero temperature is a strict low-energy quantity, in that $g(B) = \frac{\pi\Gamma}{2} \sum_{\sigma} A_{\sigma}(\omega = 0; B, T = 0)$ requires the spec-

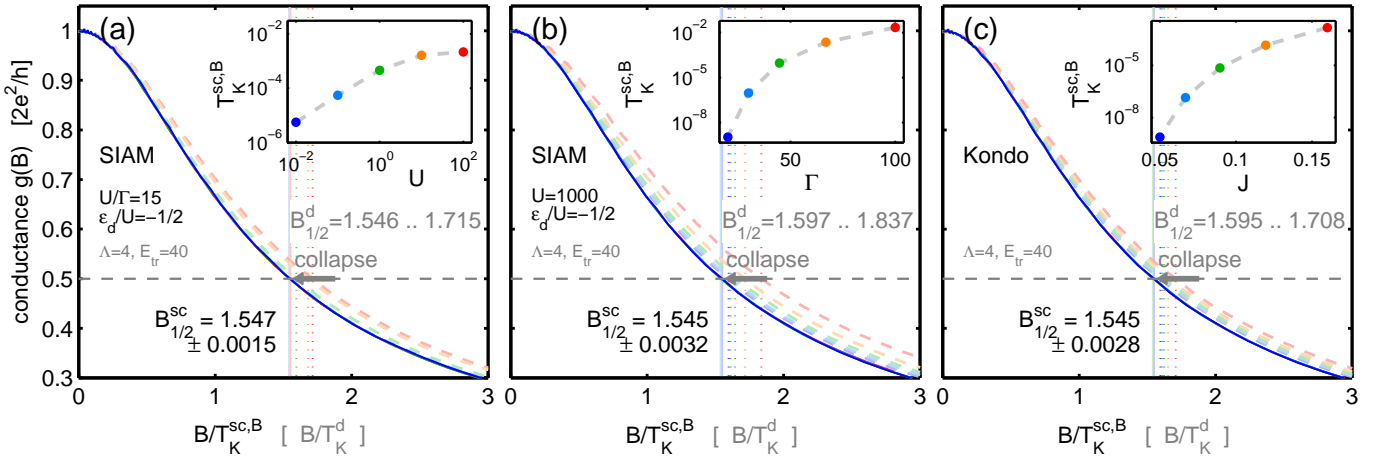


Figure 3. (Color online) Linear conductance vs. magnetic field at $T = 0$ for the SIAM (left and center panel), as well as for the Kondo model (right panel). Again the insets indicate the respective parameter setting of the lines in the main panels. Analogous to the analysis in Fig. 2(d-f), here the main panels show the static linear conductance $g(B)$ vs. B/T_K^d (non-universal; dashed faint lines, but color match with symbols of inset otherwise) and vs. $B/T_K^{sc,B}$ (solid lines) which demonstrate universal scaling. With $B_{1/2}$ the magnetic field where $g(B)$ passes through 1/2, in units of T_K^d this changes from $B_{1/2}^d \equiv B_{1/2}/T_K^d = 1.84$ down to 1.55 for given data [indicated by the vertical dotted lines with their individual range specified with each panel (gray text at center right in each panel)]. In units of $T_K^{sc,B}$ this range collapses to the value $B_{1/2}^{sc} \equiv B_{1/2}/T_K^{sc} = 1.55$ to within relative uncertainties of clearly less than 1% for all three cases [panels d-f; indicated by vertical solid light lines with the range $T_{1/2}^{sc}$ specified by the black text]. Using $\Lambda = 4$ and $E_{tr} = 40$ as indicated, the data is considered fully converged (regarding minor variations for significantly lower $E_{tr} \lesssim 10$ and thus much faster calculations, see caption to Fig. 2).

tral function evaluated at $\omega = 0$ only. As a consequence, its sensitivity on finite bandwidth is minimal (cf. App. A). This already suggests that in given case where the Hamiltonian is *altered* by a finite external parameter, universal scaling is not governed by the same T_K^{sc} as introduced in Eq. (3). Instead, through the Landauer formula, which in given case implies $\pi\Gamma \cdot A_\sigma(\omega = 0; B, T = 0) = \sin^2(\varphi_\sigma(B))$, the conductance can be directly linked to the spin-dependent low-energy phase shifts φ_σ of the entire system. For given particle-hole symmetric case, these can be written as $\varphi_\sigma(B) = \frac{\pi}{2} + \delta_\sigma(B)$ where for $|B| \ll T_K^{(FS)}$, $\delta_\sigma(B) \equiv \sigma\pi B/(4T_K^{FS})$ [cf. Eq. (5)] with $\sigma \in \{\uparrow, \downarrow\} \equiv \pm 1$. This directly identifies T_K^{FS} as defined in Eq. (4) as the relevant Kondo temperature for universal scaling. Specifically, one obtains,

$$g(B) = \frac{1}{2} \sum_{\sigma} \sin^2(\varphi_\sigma) \simeq \frac{1}{2} \sum_{\sigma} (1 - \frac{1}{2}\delta_\sigma^2)^2 \simeq 1 - \left(\frac{\pi B}{4T_K^{FS}}\right)^2 \equiv 1 - c_T \left(\frac{B}{\pi T_K^{FS}}\right)^2 \quad (11)$$

with $c_T \equiv \frac{\pi^4}{16}$ the well-known Fermi-liquid coefficient w.r.t. temperature for Kondo impurities.⁷⁻¹⁰

The scaling of the linear conductance $g(B)$ with T_K^{FS} is demonstrated in Fig. 3 for values of B that stretch well beyond the quadratic regime in Eq. (11). The analysis in Fig. 3 is completely analogous to Fig. 2(d-f), except that here the dependence is on the magnetic field. Consistent with the earlier analysis, the data for the SIAM with smallest $U = 0.01$ in Fig. 3(a) already closely resembles

the scaling limit. In contrast, the curves for the Kondo model in Fig. 3(c) even for the smallest coupling J with its extremely small T_K still do not strictly represent the scaling limit.

Above scaling analysis for $g(B)$ has major consequences for the extraction of the Fermi-liquid coefficient c_B , defined by $g(B) \simeq 1 - c_B(B/T_K)^2$ for $B \ll T_K$ at $T = 0$.⁷⁻¹⁰ Above analysis suggests that the Kondo scale, that needs to be considered for an accurate evaluation of c_B in a practical setting, is T_K^{FS} . This then again resembles the scaling limit while, nevertheless, it allows to use finite or narrow bandwidth in ones analysis provided that $T_K \lesssim 10^{-2}$ (in units of D as always).

III. SUMMARY AND OUTLOOK

In summary an adapted scheme for the calculation of the local susceptibility has been introduced which, at zero temperature, allows to define a proper universal Kondo scale T_K^{sc} . The latter fully respects scaling of measured low-energy properties such as Kondo related features. A distinction needs to be made between dynamical or temperature dependent quantities which are described by the same fixed Hamiltonian (T_K^{sc}), as compared to dependence on external parameters which directly enter the Hamiltonian, such as magnetic field ($T_K^{sc,B}$). The corrections to the commonly used T_K based on the local susceptibility χ_0^d have been summarized in Tbl. I. For the parameter sets analyzed in this paper, these corrections

range from about 0 to 10% (which become about twice as large still for Fermi liquid coefficients), yet vanish in the scaling limit.

The effect of finite bandwidth on the Kondo scale was discussed, while assuming a featureless hybridization otherwise. Proper scaling was demonstrated for the SIAM in a broad parameter regime, with the interaction U ranging from much smaller to much larger than the bandwidth D . The latter large- U limit then also was shown to smoothly connect the SIAM to the Kondo model. Essentially, this is the numerical equivalent of the Schrieffer-Wolff transformation without actually making any approximation.²⁴ By construction, the effects of finite bandwidth are clearly most prominent in the large- U limit ($U \gg D$), and as a consequence also affect most strongly the Kondo model itself. The discussion of a universal low-energy scale for specific model parameters away from the abstract true Kondo scaling limit with the bandwidth by far the largest energy is important in the experimental context, but also in the numerical context by choosing a parameter regime where simulations can be performed more efficiently (e.g. Kondo model vs. SIAM). The explicit analysis and discussion of the universal Kondo scale applied to Fermi-liquid coefficients is beyond the scope of this paper, and will be published elsewhere.

Finally, it is pointed out that the impurity contribution to the specific heat, $c_V(T)$, essentially also has the structure of a susceptibility, namely the response in energy at the impurity due to an increase in the external parameter T , i.e. the temperature. The analogies remain vague, though, since temperature is special as compared to other external parameters such as magnetic field as it enters in the Boltzmann distribution for thermal statistics. Moreover, it is also unclear a priori whether and to what extent to associate the coupling term \hat{H}_{cpl} with the impurity or the bath. Nevertheless, an approximate expression for the impurity contribution to the specific heat can be evaluated by computing $c_V(T) \simeq \frac{d}{dT} \langle \hat{H}_{\text{imp}} + \frac{1}{2} \hat{H}_{\text{cpl}} \rangle_T$.²⁹ In contrast to [29], however, which computes $c_V(T)$ by the explicit numerical derivative w.r.t. temperature, the latter can be fully circumvented along the lines of the mixed susceptibility χ^{FS} discussed above by directly computing the plain thermal expectation value $\beta \langle \hat{H}_{\text{imp}} + \frac{1}{2} \hat{H}_{\text{cpl}} | \hat{H}_{\text{tot}} \rangle_T = \beta^2 \langle (\hat{H}_{\text{imp}} + \frac{1}{2} \hat{H}_{\text{cpl}}) \hat{H}_{\text{tot}} \rangle_T$ within the fdm-NRG framework [see App. C 2 for details].

ACKNOWLEDGMENTS

We want to thank Oleg Yevtushenko, Herbert Wagner, and Jan von Delft for fruitful discussions, and also Theo Costi and Mikhail Pletyukhov for their comments on the manuscript. This work has received support from DFG (TR-12, SFB631, NIM, and WE4819/1-1).

Appendix A: Motivation for scale preserving susceptibility at $T = 0$

The definition of the magnetic susceptibility $\chi^d(T)$ in Eq. (1) is typically computed through its spectral function $\chi''(\omega) \equiv -\frac{1}{\pi} \text{Im} \chi^R(\omega)$, having $\chi(\omega) \equiv \chi'(\omega) - i\pi \chi''(\omega)$ [for simplicity, the following discussion only refers to the static local impurity susceptibility $\chi^d(T)$, hence the superscript d will be skipped for readability]. This spectral function is given by

$$\begin{aligned} \chi''(\omega) &= \int \frac{dt}{2\pi} e^{i\omega t} \chi(t) \\ &= \sum_{a,b} (\rho_a - \rho_b) |\hat{S}_z^d|_{ab}^2 \delta(\omega - E_{ab}), \end{aligned} \quad (\text{A1})$$

with $\chi(t) \equiv \langle [\hat{S}_z(t), \hat{S}_z] \rangle_T \equiv \chi^>(t) - \chi^<(t)$, corresponding to the two terms of the commutator, respectively. The last line in Eq. (A1) provides the Lehmann representation of $\chi''(\omega)$, with a and b complete many-body eigenbasis sets, having $\rho_a = \frac{1}{Z} e^{-\beta E_a}$ and $E_{ab} \equiv E_b - E_a$. Hence with $\chi(\omega) = \chi'(\omega) - i\pi \chi''(\omega)$, the static spin susceptibility $\chi(T)$ is obtained through Kramers-Kronig relations (Hilbert transform),

$$\chi(T) = \lim_{\omega \rightarrow 0} \text{P} \int \frac{\chi''(\omega')}{\omega - \omega'} d\omega' = -\text{P} \int \frac{\chi''(\omega')}{\omega'} d\omega', \quad (\text{A2})$$

with P indicating principal value integral [for finite discrete systems, this skips all energetically degenerate terms in Eq. (A1) with $E_a = E_b$; the implications of the terms $E_a = E_b$ for finite-size systems or for preserved operators are discussed in App. B]. Note that even though $\chi_0 \equiv \lim_{T \rightarrow 0} \chi(T)$ describes a low-energy property, through Eq. (A2), it requires dynamical information from all frequencies. In contrast, the mixed impurity susceptibility in Eq. (4) results in the plain expectation value $\chi^{\text{FS}}(T) = \beta \langle \hat{S}_z^{\text{tot}} \hat{S}_z^d \rangle_T$. At $T = 0$, this corresponds to a ground-state expectation value. Consequently, this quantity is static and does not explore the dynamics of the system, and hence strictly focuses on the low-energy sector. For this reason, as pointed out in the main text, this quantity exactly reflects, for example, the phase-shifts experienced by the electrons of the bath in the low-energy fixed point spectrum.

Nevertheless, this mixed impurity susceptibility is still insufficient for the evaluation of a proper scale-preserving susceptibility. In order to proceed, while still insufficient, it is instructive to consider the effects of spectral moments (next section). This will be followed by the actual motivation of the scale-preserving susceptibility based on the plain non-interacting resonant level model.

1. Effects of spectral moments

The Kramers-Kronig or Hilbert transform in Eq. (A2), in a sense, corresponds to the spectral moment with

$n = -1$ [by using the spectral weight $(\omega')^n$ within the integral]. This clearly weights small frequencies more strongly. Hence this emphasizes the low-energy sector while, nevertheless, it weakly reaches out towards large energies. This becomes more pronounced still for $n = 0$, which simply corresponds to the spectral sum rule,

$$I \equiv \int \chi^>(\omega') d\omega' = \int (1 - f(\omega')) \chi''(\omega') d\omega' \\ = \langle (\hat{S}_z^d)^2 \rangle_T \lesssim \frac{1}{4}, \quad (\text{A3})$$

with $f(\omega)$ the Fermi function. For $T = 0$, this exactly describes the area underneath the spin-spin correlation function $\chi''(\omega)$ for positive or, up to a sign, for negative frequencies [cf. Fig. 1; the integral over the entire $\chi^d(\omega)$ for all frequencies yields zero by the antisymmetry of $\chi^d(\omega)$].

For the SIAM in the local-moment (Kondo) regime, the value of the integral in Eq. (A3) at $T = 0$ is close to its upper bound, $I_0^{\text{SIAM}} \lesssim 0.25$, with minor variations of $\lesssim 10\%$ depending on the specific model parameters. For the Kondo model (which represents the large- U limit of the SIAM, i.e. $U \gg D$), by construction, the sum-rule in Eq. (A3) exactly yields the upper bound $I_0^{\text{Kondo}} = 1/4$.

At $T = 0$, the scaling of the spectral data $\chi''(\omega)$ by $\chi_0 = \lim_{T \rightarrow 0} \chi(T)$ ensures that the height of $\chi''(\omega)$ is properly normalized [e.g. see Fig. 1, all panels]. Since the area underneath $\chi''(\omega)$ is (roughly) conserved, scaling of the frequency ω by χ_0^{-1} leads to approximate scaling (left panels of Fig. 1). Specifically, since for the Kondo model, the area is exactly preserved (see above), the remaining horizontal variations in Fig. 1(c) *must be due to finite bandwidth*. In conclusion, the sum-rule in Eq. (A3) is not particularly useful for a proper scale-preserving local susceptibility. This is not surprising, considering that it represents the spectral moment $n = 0$, and hence is strongly susceptible to effects of finite bandwidth (for the Kondo model this means that, while the area in Eq. (A3) is preserved, there can be a shift of spectral weight from the band edge to low-energy Kondo regime and vice versa, hence spoiling scaling of the low-energy Kondo features). Higher spectral moments will make things even worse. Hence this route appears ill-suited for the search of a scale-preserving local susceptibility at $T = 0$.

2. Motivation through the non-interacting SIAM

The scale-preserving susceptibility proposed in the main text was also tested successfully for the asymmetric SIAM, as well as in the limit $U \rightarrow 0$ at finite Γ , i.e. the plain non-interacting resonant level model. Even there, the proposed χ_0^{sc} still nicely allowed for scaling of low-energy features, such as the impurity spectral function $A(\omega) \equiv -\frac{1}{\pi} \text{Im} G_d(\omega)$, as long as the low-energy scale (here Γ) is clearly smaller than the bandwidth, i.e. $\Gamma \lesssim 10^{-2}$. The reason for this will be explained in what follows. Considering that the general impurity

Green's function for an interacting system can be written as $G_d(\omega) = [\omega - \varepsilon_d - \Delta(\omega) - \Sigma(\omega)]^{-1}$, with $\Sigma(\omega)$ the impurity self-energy, the discussion of the effects of finite bandwidth on the hybridization function $\Delta(\omega)$ below may serve as a more general motivation, indeed, for the definition of a scale preserving susceptibility. In particular, as it is demonstrated in the main paper, the result can also be nicely applied to interacting systems.

For the non-interacting case, with $\sigma \in \{\uparrow, \downarrow\} \equiv \{\pm 1\}$, the spin susceptibility reduces to the impurity charge-susceptibility for the spinless model. With $\langle \hat{S}_z^d \rangle_T = 0$, one has

$$\chi^d(T) = \frac{1}{4} \sum_{\sigma, \sigma'} \sigma \sigma' \cdot \underbrace{\langle \hat{n}_\sigma \| \hat{n}_{\sigma'} \rangle_0}_{\propto \delta_{\sigma \sigma'}} = \frac{1}{2} \langle \hat{n}_{(\sigma)} \| \hat{n}_{(\sigma)} \rangle_0 \\ \equiv -\frac{1}{2} \lim_{\omega \rightarrow 0} \chi^c(\omega), \quad (\text{A4a})$$

[regarding the sign in the last line, see Eq. (A2)], with the charge susceptibility given by

$$\chi^c(\omega) \equiv \text{FT}(-i\vartheta(t) \langle [\hat{n}(t), \hat{n}] \rangle_T), \quad (\text{A4b})$$

with $\hat{n} \equiv \hat{d}^\dagger \hat{d}$, and FT() indicating Fourier transform. In the non-interacting case, this results in the impurity susceptibility

$$\chi^d(T) = -\frac{\partial}{\partial \varepsilon_d} \langle \hat{n} \rangle_T = \text{Im} \int \frac{d\omega}{2\pi} [G_d(\omega)]^2 f(\omega), \quad (\text{A5})$$

with $G_d(\omega)$ the impurity Green's function and $f(\omega)$ the Fermi function. This results in the correct large temperature limit, $\lim_{T \rightarrow \infty} T \chi_0(T) = \frac{1}{8}$ for arbitrary $G_d(\omega)$. The low-temperature limit is model dependent. Considering the non-interacting case, the impurity Green's function is given by $G_d(\omega) = [\omega - \varepsilon_d - \Delta(\omega)]^{-1}$, with $\Delta(\omega^+) \equiv \sum_k \frac{V_k^2}{\omega^+ - \varepsilon_k} \equiv E(\omega) - i\Gamma(\omega)$ the hybridization function. In the wide-band limit for constant $\Gamma(\omega) = \theta(D - |\omega|)\Gamma$, it follows that $E(\omega) \rightarrow 0$. The effects of finite bandwidth D manifest themselves at small frequencies ω through

$$\varepsilon_d \rightarrow \varepsilon_d + E(\omega) \simeq \tilde{\varepsilon}_d - a\omega, \quad (\text{A6a})$$

with $\tilde{\varepsilon}_d \equiv \varepsilon_d + E(0)$ and $a \equiv -\left. \frac{d}{d\omega} E(\omega) \right|_{\omega=0} \sim \Gamma/D \ll 1$ some dimensionless small constant (note that for the particle-hole symmetric resonant level model with constant Γ , one has $a \geq 0$). This leads to the scaling

$$\omega \rightarrow \tilde{\omega} \equiv (1 - a)\omega. \quad (\text{A6b})$$

of the frequency in $G_d(\omega)$ in Eq. (A5) (interestingly, this may be interpreted more generally in an interacting context as the scaling of frequency by the quasi-particle weight z^{17}). Therefore far away from the bandwidth, $|\omega| \ll D$, the impurity spectral function appears slightly *stretched* along the frequency axis while preserving its height. Overall, however, the line shape for small frequencies *remains unaltered* up to proper scaling factors.

With respect to frequency, Eq. (A6b) suggests the *increased* energy scale $T_K^{\text{sc}} = T_K^\infty / (1 - a)$ relative to T_K^∞

which, to lowest order in a , represents the energy scale in the wide-band limit. Remembering that $\chi_0 \propto T_K^{-1}$ represents an inverse energy scale, one obtains

$$\chi_0^{\text{sc}}(D) = (1-a)\chi_0^\infty, \quad (\text{A6c})$$

with $\chi_0^{\text{sc}}(D)$ the scale-preserving local susceptibility at given finite bandwidth, and $\chi_0^\infty \equiv 1/(4T_K^\infty)$.

On the other hand, at $T = 0$, the Fermi function in Eq. (A5) is unaffected by the scaling $\omega \rightarrow \tilde{\omega}$, such that the overall integral in Eq. (A5) may be rewritten in terms of $\tilde{\omega}$, resulting in

$$\chi_0^{\text{d}}(D) \simeq \frac{1}{1-a}\chi_0^\infty \stackrel{(\text{A6c})}{=} \left(\frac{1}{1-a}\right)^2 \chi_0^{\text{sc}}(D). \quad (\text{A7})$$

With $a > 0$, this shows that $\chi_0^{\text{d}}(D)$ overestimates the scale-preserving susceptibility $\chi^{\text{sc}}(D)$ for given finite bandwidth D .

The mixed susceptibility now allows to determine and subsequently eliminate the scale factors $(1-a)$. With

$$\begin{aligned} \chi^{\text{FS}}(T) &= \int_0^\beta d\tau \langle \hat{S}_z^{\text{d}}(\tau) \hat{S}_z^{\text{tot}} \rangle = \beta \langle \hat{S}_z^{\text{d}} \hat{S}_z^{\text{tot}} \rangle \\ &= \frac{\beta}{2} (\langle \hat{n} \hat{N} \rangle - \langle \hat{n} \rangle \langle \hat{N} \rangle), \end{aligned} \quad (\text{A8a})$$

the last line again already refers to a spinless model, with $\hat{n} \equiv \hat{d}^\dagger \hat{d}$ the number of particles at the impurity and \hat{N} the total number of particles in the system. In the non-interacting case with $A(\omega) \equiv -\frac{1}{\pi} \text{Im} G_d(\omega)$ the impurity spectral function, this becomes

$$\chi^{\text{FS}}(T) = \frac{1}{2} \int d\omega A(\omega) (-f'(\omega)). \quad (\text{A8b})$$

In the limit $T \rightarrow 0$, this yields $\chi_0^{\text{FS}} = A(0)/2$. While $A(\omega)$ depends on the rescaled frequency $\omega \rightarrow (1-a)\omega$, as discussed above, this is irrelevant here since $A(\omega)$ is evaluated at $\omega = 0$. In the wide-band limit of a featureless bath, i.e. constant hybridization Γ , Eq. (A5) exactly agrees with Eq. (A8b). Together with the fact that χ_0^{FS} does not explicitly depend neither on the bandwidth nor dynamically on finite frequency, this allows to identify $\chi_0^{\text{FS}} = \chi_0^\infty$ even at *finite* D .

Using Eq. (A7), the effects of finite bandwidth on $\chi_0^{\text{sc}}(D)$ to lowest-order in a are thus summarized by

$$\chi_0^{\text{sc}}(D) = (1-a)^2 \chi_0^{\text{d}}(D) \simeq (1-2a)\chi_0^{\text{d}}(D). \quad (\text{A9})$$

The first reduction of $\chi_0^{\text{d}}(D)$ by the factor $(1-a)$ leads to χ_0^{FS} . Another reduction by the same factor leads to the desired $\chi_0^{\text{sc}}(D)$. With $a \ll 1$, this implies that the difference between $\chi_0^{\text{d}}(D)$ and χ_0^{FS} , as well as the difference between χ_0^{FS} and $\chi_0^{\text{sc}}(D)$ are the same to lowest order in a , and are given by the first equality in Eq. (A7), $a\chi_0^{\text{d}}(D) \simeq \chi_0^{\text{d}}(D) - \chi_0^{\text{FS}}$. Together with the last term in Eq. (A9) then, one obtains the final expression for the scale-preserving local susceptibility,

$$\chi_0^{\text{sc}}(D) = 2\chi_0^{\text{FS}} - \chi_0^{\text{d}}(D), \quad (\text{A10})$$

in agreement with Eq. (3b) in the main paper.

Appendix B: Impurity susceptibility and finite size effects

Consider the Lehmann representation of the generic impurity susceptibility given by the last term in Eq. (7),

$$\begin{aligned} \langle \hat{X} \parallel \hat{Y} \rangle_T &= \sum_{a,b} \frac{e^{-\beta E_a}}{Z} (\delta X)_{ab} (\delta Y)_{ba} \frac{1-e^{-\beta E_{ab}^\dagger}}{E_{ab}^\dagger} \quad (\text{B1a}) \\ &= \underbrace{\sum_{a \neq b} \frac{e^{-\beta E_a} - e^{-\beta E_b}}{Z} \frac{X_{ab} Y_{ba}}{E_{ab}^\dagger}}_{\equiv \langle \hat{X} \parallel \hat{Y} \rangle_T^{(R)}} + \underbrace{\beta \sum_a \frac{e^{-\beta E_a}}{Z} (\delta X)_{aa} (\delta Y)_{aa}}_{\equiv \langle \hat{X} \parallel \hat{Y} \rangle_T^{(\delta)}}. \end{aligned} \quad (\text{B1b})$$

Here a and b represent complete many-body eigenbasis sets, i.e. $\hat{H}|a\rangle = E_a|a\rangle$ with $E_{ab} \equiv E_b - E_a$, and the Boltzmann distribution $\rho_a = e^{-\beta E_a}/Z$ (note that $(\delta X)_{aa} = X_{aa} - \langle \hat{X} \rangle_T \neq 0$ in general). In the first line the positive infinitesimal, $E_{ab}^\dagger \equiv E_{ab} + i0^+$, was added for convenience to correctly deal with the case $E_a = E_b$ (the sign of the infinitesimal imaginary part is initially actually irrelevant here). By splitting off the terms $a = b$ of the sum in Eq. (B1a) into the correction $\langle \hat{X} \parallel \hat{Y} \rangle_T^{(\delta)}$, the first term in Eq. (B1b) then translates into the Kubo formula for linear response $\langle \hat{X} \parallel \hat{Y} \rangle_T^{(R)}$ based on the retarded response function. By the way the specific infinitesimals are chosen, actually all degenerate terms $E_a = E_b$ drop out of the first term (principal value integral in the continuum's limit), which therefore ignores accidental degeneracies, i.e. degeneracies beyond strict internal multiplet degeneracies due to symmetry which are included with the second term. As a consequence, the sum in the first term can be relaxed back to all a, b including $a = b$. Furthermore, the correction $\langle \hat{X} \parallel \hat{Y} \rangle_T^{(\delta)}$ in Eq. (B1b) is relevant only if the spin states of the states a are sufficiently long-lived. In the extreme case $\hat{X} = \hat{Y} = \hat{S}_z^{\text{tot}}$, the first term $\langle \hat{X} \parallel \hat{Y} \rangle_T^{(R)}$ in Eq. (B1) is strictly zero, and therefore the entire susceptibility is carried by the second term. In contrast, for the case that the Hamiltonian does not commute with \hat{X} say, in the thermodynamic limit one expects that $X_{aa} \rightarrow 0$ and the second term in Eq. (B1) vanishes. In this case linear response is safe using either Kubo formula or the imaginary-time Matsubara susceptibility. However, in the presence of discretized finite-size systems, $X_{aa} \neq 0$ can become a significant contribution nevertheless! In this case, both contributions in Eq. (B1) must be included.

1. Limit of large temperature for finite system

For a finite system in the limit $\beta|E_{ab}| \ll 1$, Eq. (B1a) becomes

$$\begin{aligned} \lim_{T \rightarrow \infty} \langle \hat{X} \| \hat{Y} \rangle_T &\simeq \sum_{a,b} \frac{e^{-\beta E_a}}{Z} (\delta X)_{ab} (\delta Y)_{ba} \underbrace{\frac{1-(1-\beta E_{ab}^+)}{E_{ab}^+}}_{=\beta} \\ &= \beta \lim_{T \rightarrow \infty} \langle \delta \hat{X} \cdot \delta \hat{Y} \rangle_T = \beta \lim_{T \rightarrow \infty} [\langle \hat{X} \hat{Y} \rangle_T - \langle \hat{X} \rangle_T \langle \hat{Y} \rangle_T], \end{aligned} \quad (\text{B2})$$

which is equivalent to the situation where either operator \hat{X} or \hat{Y} actually commutes with the Hamiltonian! This again serves to emphasize the importance of both terms in the evaluation of the impurity susceptibility in Eq. (B1) in any numerical setting for a finite system, even if both, \hat{X} and \hat{Y} , do not commute with the Hamiltonian. While in the case of small T the last term in Eq. (B1b) may be negligible, it gains relative importance with increasing temperature, to the extent, that for a finite system with $T \rightarrow \infty$ comparable weight is carried by both terms in Eq. (B1b) [note that for large T , $\langle \hat{X} \| \hat{Y} \rangle_T^{(R)} \propto 1/T$, while the $1/T$ behavior of the correction $\langle \hat{X} \| \hat{Y} \rangle_T^{(\delta)}$ is caused by the leading β ; cf. explicit NRG analysis in Fig. 4 below].

2. Impurity susceptibility at large temperatures

In the limit $T \rightarrow \infty$, the thermal density matrix is fully mixed and hence independent of the eigenbasis of the actual Hamiltonian. The thermal average therefore can be reduced to the thermal average within the impurity space alone. Therefore with $\hat{S}_z^{\text{tot}} \equiv \sum_n \hat{S}_z^{(n)}$ summed over all (Wilson) sites n including the impurity, having $\langle \hat{S}_z^{\text{d}} \rangle_T = 0$, Eqs. (2-4) reduce to the same asymptotic form

$$\begin{aligned} (T\chi)_\infty &\equiv \lim_{T \rightarrow \infty} T\chi^{\text{sc}}(T) \simeq \lim_{T \rightarrow \infty} \langle \hat{S}_z^{\text{d}} \| \hat{S}_z^{\text{d}} \rangle_T \\ &= \frac{1}{d_i} \sum_{\sigma_i} (S_{z,\sigma_i}^{\text{d}})^2, \end{aligned} \quad (\text{B3})$$

where the impurity is described by the state space σ_i of dimension d_i that also diagonalizes \hat{S}_z^{d} . For a Kondo impurity, or also for an Anderson impurity in the case $T_K \ll D \ll T \ll U$, this implies $\chi_\infty = \frac{1}{4T}$ [this also may be taken as a motivation for the definition of the Kondo temperature $T_K = \frac{1}{4\chi_0}$ in Eq. (1) in the opposite limit of $T \rightarrow 0$; more generally still, for an impurity of spin S one obtains $(T\chi)_\infty = \frac{S(S+1)}{3}$]. On the other hand, for an Anderson impurity with $T \gg U$, one obtains $\chi_\infty = \frac{1}{8T}$ due to the enlarged accessible local state space³⁰ [see also Figs. 2(a-b)].

3. Implications for the NRG

Above considerations are clearly relevant for numerical simulations such as the NRG. There the effective length of the Wilson chain becomes ever shorter for calculations with increasing temperature (automatically so in case of fdm-NRG).^{23,25} In case of NRG, the interplay between finite-size effects and large temperatures can therefore be considered enhanced.

The two contributions to the static susceptibility in Eq. (B1) are analyzed in detail in Fig. 4 for the data in Fig. 2 of the main paper. From the log-log plots in the lower panels it is clearly seen that $T\chi^\delta \propto 1/T^2$ for $T \ll T_K$ [in contrast to $T\chi^R \propto 1/T$], and hence becomes negligible in the limit $T \rightarrow 0$. Nevertheless, once T increases and becomes comparable to T_K , the correction $T\chi^R(T)$ becomes sizable. While the two contributions to the static susceptibility in Eq. (B1) show rather irregular behavior individually, as seen in Fig. 4, their sum yields a smooth physically meaningful curve.

In practice, when computing the first term in Eq. (B1b) as standard susceptibility within linear response (Kubo formula), the second term shows up in a disguised manner as $\delta(0)$ contribution with opposite sign for $\omega = 0^\pm$. This may be collected in the smallest frequency bin for positive and negative frequencies, respectively, when collecting the discrete data. While these $\delta(0)$ contributions drop out of the principal value summation in the Kramers-Kronig transformation, nevertheless, it it represents, and thus can be simply used to subsequently evaluate the correction given by the last term in Eq. (B1b).

Appendix C: Calculation of the mixed susceptibility $\chi^{\text{FS}}(T)$ within fdm-NRG

Given that the total spin operator \hat{S}_z^{tot} commutes with the Hamiltonian, the mixed susceptibility $\chi^{\text{FS}}(T) \equiv \langle \hat{S}_z^{\text{d}} \| \hat{S}_z^{\text{tot}} \rangle_T$ in Eq. (4) can be evaluated in a simple and cheap manner, as it reduces to the plain set of expectation values, $T\chi^{\text{FS}}(T) = \langle \hat{S}_z^{\text{tot}} \hat{S}_z^{\text{d}} \rangle_T - \langle \hat{S}_z^{\text{tot}} \rangle_T \langle \hat{S}_z^{\text{d}} \rangle_T$. This includes one local operator \hat{S}_z^{d} and one global operator, the total spin operator $\hat{S}_z^{\text{tot}} \equiv \sum_n \hat{S}_z^{(n)}$ which is given by the sum of local spins $\hat{S}_z^{(n)}$ associated with site n along the Wilson chain including the impurity, say, at $n = -1$. Being interested in the magnetic susceptibility at zero magnetic field, it follows $\langle \hat{S}_z^{\text{tot}} \rangle_T = \langle \hat{S}_z^{\text{d}} \rangle_T = 0$. The remaining quantity then,

$$T \cdot \chi^{\text{FS}}(T) = \langle \hat{S}_z^{\text{tot}} \hat{S}_z^{\text{d}} \rangle_T = \text{tr}[\hat{\rho}(T) \cdot \hat{S}_z^{\text{tot}} \hat{S}_z^{\text{d}}], \quad (\text{C1})$$

is a simple intrinsic quantity that is solely related to the impurity. In given case only a single sum over a complete many-body eigenbasis a suffices, with the Lehmann representation of Eq. (C1) given by

$$T \cdot \chi^{\text{FS}}(T) = \sum_a \frac{e^{-\beta E_a}}{Z} S_{z,a}^{\text{tot}} \left(\hat{S}_z^{\text{d}} \right)_{aa}, \quad (\text{C2})$$

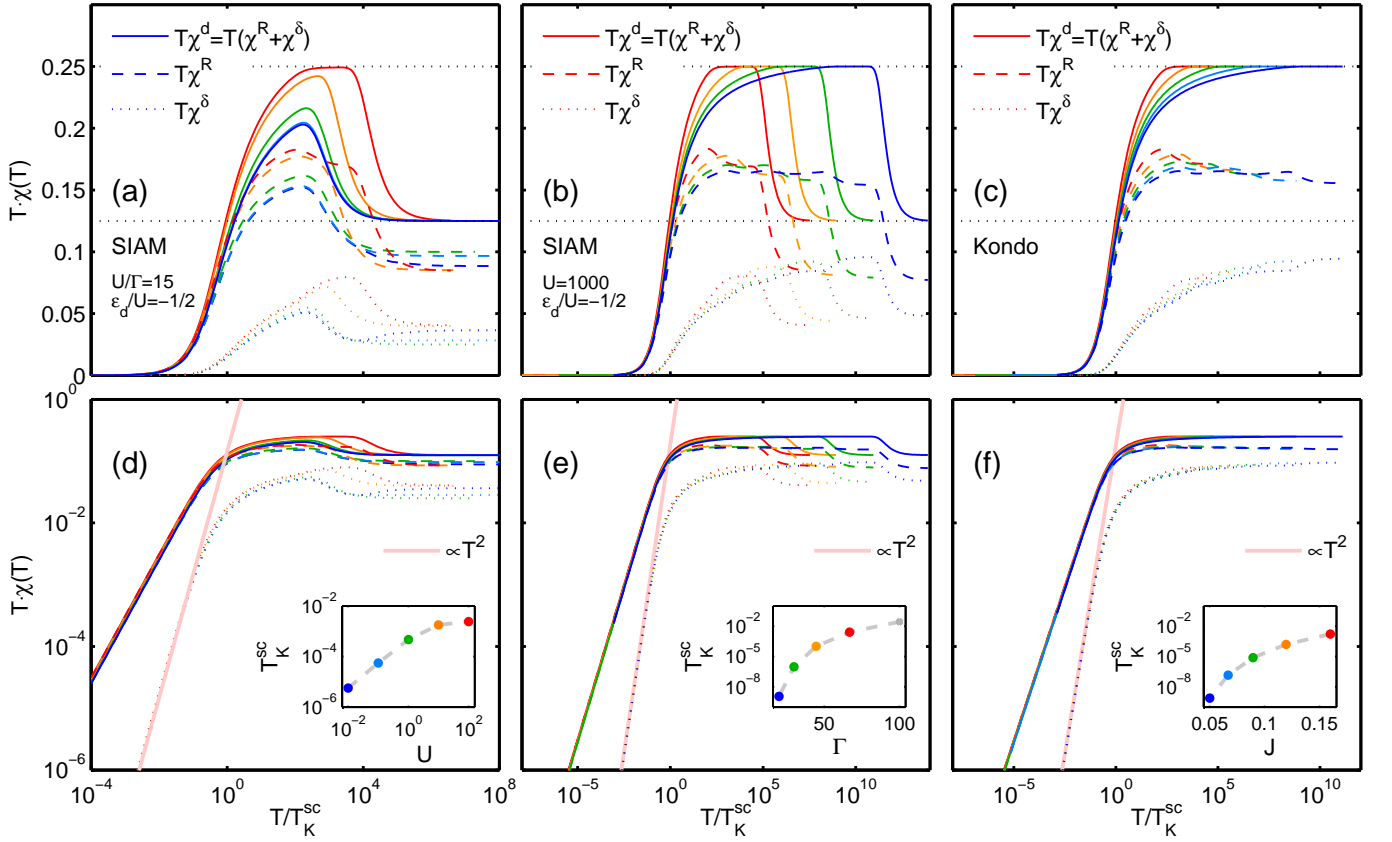


Figure 4. (Color online) Contributions to the impurity susceptibility χ^d as in Eq. (B1) for the data in Fig. 2 in the main paper [panels (a-c) have exactly the same parameter setting as Fig. 2(a-c)]. The lower panels replicate the same data as in the upper panel, yet switching to a log-scale also on the vertical axis. The thick light solid line corresponds to a plain power-law fit, suggesting that the correction $T\chi^\delta$ decays like $1/T^2$, hence becomes irrelevant in the limit $T \rightarrow 0$. The insets in the lower panels have been replicated from Fig. 2 to indicate the parameter setting.

where $\hat{H}|a\rangle \equiv E_a|a\rangle$. By construction, the full thermal density matrix as well as the total spin operator S_z^{tot} are strictly diagonal, with the matrix elements given by $[S_z^{\text{tot}}]_{aa'} = \delta_{aa'} S_{z,a}^{\text{tot}}$ and $[\hat{\rho}(T)]_{aa'} = \delta_{aa'} e^{-\beta E_a} / Z$, respectively, with $Z(T) \equiv \sum_a e^{-\beta E_a}$ the grand-canonical partition function.

In what follows, the complete basis set a is given by the iteratively discarded state spaces generated by the NRG,²⁶ i.e. $|a\rangle \rightarrow |se\rangle_n^D \equiv |s\rangle_n^D \otimes |e\rangle_n$ with $s_n \in D$ a discarded state at iteration n and e_n the environment w.r.t. iteration n , i.e. the full state space for the remainder of the Wilson chain $n < n' \leq N$ with N the final length of the Wilson chain considered. The resulting full thermal density matrix (fdm) is given by^{23,25}

$$\hat{\rho}(T) = \sum_n w_n(T) \hat{\rho}_n^D(T), \quad (\text{C3})$$

where $w_n(T)$ is a well-defined temperature-dependent weight distribution along the Wilson chain that is peaked near the energy scale of temperature. The operators $\hat{\rho}_n^D$ are normalized thermal density matrices within the discarded state space of iteration n (the sum over the envi-

ronment of the remaining iterations, resulting in the degeneracy factor d^{N-n} with d the dimension of the local state space of a single Wilson site, has been already properly included in the weight distribution w_n).^{23,25} With the full thermal density matrix a scalar operator, all entries in Eq. (C3) are block-diagonal. In particular, being initialized within the discarded (eigen-) state space at iteration n itself, all $\hat{\rho}_n^D$ are strictly diagonal.

Now, assuming that also \hat{S}_z^{tot} commutes with the Hamiltonian, it is also block diagonal. Using the complete basis set $|se\rangle_n^D \equiv |s\rangle_n^D \otimes |e\rangle_n$, in the expectation value in Eq. (C2) for the mixed susceptibility, the environment is traced over. Specifically with

$$\hat{S}_z^{\text{tot}} \equiv \sum_n \hat{S}_z^{(n)} = \underbrace{\sum_{n' \leq n} \hat{S}_z^{(n')}}_{\equiv \hat{S}_z^{n, \text{tot}}} + \underbrace{\sum_{n' > n} \hat{S}_z^{(n')}}_{\equiv \hat{S}_z^{e, \text{tot}}},$$

the total spin of the entire Wilson chain splits into two parts w.r.t. a given iteration n , the total spin up to and including site n , and the total spin for the remainder of the chain. The corresponding matrix elements are given

by (note that the degeneracy factor d^{N-n} has been already included with the weight distribution w_n and is thus compensated in the following expression),

$$\begin{aligned} & \frac{1}{d^{N-n}} \sum_{e_n} \langle se | \hat{S}_z^{\text{tot}} | s' e \rangle_n = \\ & = \delta_{ss'} S_{z,s}^{n,\text{tot}} + \delta_{ss'} \sum_{n' > n} \frac{1}{d} \underbrace{\sum_{\sigma_{n'}} \langle \sigma_{n'} | \hat{S}_z^{(n')} | \sigma_{n'} \rangle}_{= \langle \hat{S}_z^{(n')} \rangle_{\infty=0}}, \end{aligned}$$

where $\sigma_{n'}$ spans the d -dimensional local Hilbert space of Wilson site n' . The last term represents the fully mixed average of the local spin for a given site n' , i.e. corresponding to an effective $T = \infty$, and thus vanishes identically by symmetry. Overall, this implies that at iteration n , only the total spin $\hat{S}_z^{n,\text{tot}}$ up to and including site n needs to be considered. Therefore the mixed susceptibility in Eq. (C1) can be evaluated in the NRG context as follows,

$$\begin{aligned} T \cdot \chi^{\text{FS}}(T) &= \sum_n w_n(T) \text{tr} \left[\underbrace{\rho_n^D(T) S_z^{n,\text{tot}} S_z^{\text{d}}}_{= \sum_{s \in D_n} \rho_{n,s}(T) S_z^{n,\text{tot}}(S_z^{\text{d}})_{ss}} \right], \quad (\text{C4}) \end{aligned}$$

where the trace runs over the discarded state space of iteration n as indicated. Here the notation of the operators without hats indicates that they already correspond to the matrix representations in the basis $s \in D_n$, i.e. the discarded states at iteration n . The computationally most expensive part for the result Eq. (C4) is the evaluation of the matrix elements of \hat{S}_z^{d} in the discarded state space of iteration n . From these, however, only the diagonals are required. Once computed, the calculation of $\chi^{\text{FS}}(T)$ becomes extremely fast for an arbitrary set of temperatures. It is important, though, that for the physically correct impurity susceptibility thermal averaging at $T = 0^+$ is required. Hence the Wilson chain has to be chosen long enough such that the weight distribution $w_n(T)$ clearly fits within the Wilson chain, i.e. $w_N(T) \lesssim 10^{-2}$, with N the length of the Wilson chain considered (in practice, $T \gg \omega_N$).

1. Evaluation in the presence of non-abelian symmetries

In the above discussion, the external magnetic field was applied in the z -direction. However, if the magnetic susceptibility at $B = 0$ is computed, the Hamiltonian typically possess $SU(2)$ spin symmetry. This can be taken advantage of when evaluating the mixed susceptibility above as follows. Clearly, the evaluation of the mixed susceptibility Eq. (C1) can be symmetrized w.r.t. x -, y -, and z -components,²⁴

$$T \chi^{\text{FS}}(T) = \langle \hat{S}_z^{\text{tot}} \hat{S}_z^{\text{d}} \rangle_T = \frac{1}{3} \langle \hat{S}^{\text{tot}} \cdot \hat{S}_z^{\text{d}} \rangle_T,$$

where $\hat{S} \equiv [\frac{-1}{\sqrt{2}} \hat{S}_+, \hat{S}_z, \frac{+1}{\sqrt{2}} \hat{S}_-]^T \equiv \{\hat{S}_\mu\}$ with $\mu \in \{+1, 0, -1\}$ represents the irreducible three-dimensional

spinor for the spin operator which transforms according to a spin $J = 1$ multiplet. Now every component in the spinor \hat{S}^{tot} commutes with the Hamiltonian such that \hat{S}_\pm^{tot} only raises or lowers the state index within the *same* multiplet, but never leaves a given multiplet. As a consequence, \hat{S}^{tot} is still a strictly diagonal operator in multiplet space, while the non-diagonal matrix elements within the same multiplet factorize as Clebsch-Gordan coefficients (cf. Wigner Eckart theorem). To be specific, in the presence of symmetries, the state space at each iteration n is organized using the composite index labels²⁴ $|s\rangle_n \rightarrow |Js; M\rangle_n$ where $s_{(J)}$ now labels a specific multiplet within symmetry sector J , and $M_{(J)}$ represents the S_z labels, i.e. sequences the internal state space of multiplet J . With this, the matrix elements of the total spin operators are given by

$$\begin{aligned} & \langle J'n'; M' | \hat{S}_\mu^{n,\text{tot}} | Jn; M \rangle \\ & = \delta_{JJ'} \underbrace{\delta_{nn'} \sqrt{J(J+1)}}_{\equiv \|S_J^{n,\text{tot}}\|_{nn'}} \cdot (JM' | 1\mu; JM) \end{aligned}$$

The prefactor in the reduced matrix elements $\|S_J^{n,\text{tot}}\|$ for symmetry sector J guarantees that one obtains the familiar Casimir operator,

$$\langle Jn; M' | (\hat{S}^{n,\text{tot}})^\dagger \cdot \hat{S}^{n,\text{tot}} | Jn; M \rangle = J(J+1) \delta_{MM'}. \quad (\text{C5})$$

Consequently, in the presence of $SU(2)$ spin symmetry, within the NRG the mixed susceptibility in Eq. (C4) can be rewritten as follows,

$$T \chi^{\text{FS}}(T) = \frac{1}{3} \sum_n w_n \text{tr} \left[\rho_n^D (S^{\text{d}} \cdot S^{n,\text{tot}}) \right]. \quad (\text{C6})$$

The apparent overhead in terms of the extra summation over the μ components of the spinors in $S^{\text{d}} \cdot S^{n,\text{tot}}$ is completely negligible when compared to the gain by the reduced dimensionality on the reduced matrix element, i.e. the multiplet level. First of all, it only affects Clebsch-Gordan coefficient spaces. Moreover, by inspecting the block-diagonal structure of Eq. (C6), for the specific contribution of any symmetry sector within the trace *exactly the same* Clebsch-Gordan coefficient space appears twice, in both $S_\mu^{n,\text{tot}}$ as well as S_μ^{d} . Hence, by performing the trace for the Clebsch Gordan coefficient space similar to Eq. (C5), this only adds a factor $(2J+1)$, i.e. the $3j$ -symbol, which is simply equal to the dimensionality of multiplet J . Hence the explicit contraction of the Clebsch-Gordan coefficients can be fully circumvented. In summary, the effect of non-abelian symmetries on the evaluation of the mixed susceptibility in Eq. (C6) is that (i) S^{d} can be reduced to its block-diagonal components due to the block-diagonal structure of all the remaining participants. (ii) The traced-over Clebsch-Gordan spaces together with the definition of $S^{n,\text{tot}}$ results in the combined factor $\frac{1}{3} \sqrt{J(J+1)}(2J+1)$ for symmetry sector J that can be directly multiplied onto the reduced matrix elements of S^{d} . Finally, with the Clebsch-Gordan coefficients taken care of, (iii) the remaining trace is carried out over the reduced multiplet space only.

2. Evaluation of the approximate impurity specific heat $\langle(\hat{H}_{\text{imp}} + \frac{1}{2}\hat{H}_{\text{cpl}})\hat{H}_{\text{tot}}\rangle_T$ within fdm-NRG

The impurity specific heat has a similar mathematical structure when compared to the general discussion of susceptibility above. However, since it would be a susceptibility that refers to the temperature itself as the variable physical parameter, in the presence of thermal averages, these similarities necessarily remain vague and the impurity specific heat is special. Nevertheless, as it turns out,²⁹ the impurity specific heat can also be computed through the following *local* approximation,

$$c_V(T) \simeq \frac{\partial}{\partial T_{(\text{tot})}} \langle \hat{H}_{\text{ipc}} \rangle_T = \frac{\partial}{\partial T_{\text{ipc}}} \langle \hat{H}_{\text{tot}} \rangle_T, \quad (\text{C7})$$

where $\hat{H}_{\text{ipc}} \equiv \hat{H}_{\text{imp}} + \frac{1}{2}\hat{H}_{\text{cpl}}$, with \hat{H}_{imp} and \hat{H}_{cpl} the impurity Hamiltonian and its coupling to the bath, respectively [e.g. see Eq. (9)]; here *ipc* stands for impurity plus part of the coupling to the bath]. The first expression, $\frac{\partial}{\partial T_{(\text{tot})}} \langle \hat{H}_{\text{ipc}} \rangle$, has the intuitive physical interpretation that it represents the change in energy at the impurity due to a change in the overall total temperature, where the contribution of the hybridization is shared *in equal parts* with the bath²⁹. Mathematically, this is equivalent to the second expression in Eq. (C7), $\frac{\partial}{\partial T_{\text{ipc}}} \langle \hat{H}_{\text{tot}} \rangle$, which represents the change in total energy due to a change in local temperature, i.e. with $\beta \equiv 1/T_{(\text{tot})}$ and $\hat{H}_{(\text{tot})} \equiv \hat{H}_{\text{ipc}} + \hat{H}_{\text{bpc}}$ (where *bpc* stands for bath plus remaining contribution from the coupling to the impurity),

$$\begin{aligned} e^{-\beta \hat{H}} &\equiv \exp\left(-\frac{1}{T_{(\text{tot})}}(\hat{H}_{\text{ipc}} + \hat{H}_{\text{bpc}})\right) \\ &\rightarrow \exp\left(-\frac{1}{T_{\text{ipc}}}\hat{H}_{\text{ipc}} - \frac{1}{T_{\text{bpc}}}\hat{H}_{\text{bpc}}\right), \end{aligned} \quad (\text{C8})$$

evaluated at $T_{\text{ipc}} = T_{\text{bpc}} = T_{(\text{tot})}$ *after* taking the derivative for $c_V(T)$, as indicated by the trailing subscript T in the last term of Eq. (C7).

While in [29] the derivative in Eq. (C7) was computed numerically by first computing the expectation values $\langle \hat{H}_{\text{ipc}} \rangle_T$, the derivative in Eq. (C7) can be easily expressed analytically,

$$c_V(T) = \beta^2 \left[\langle \hat{H}_{\text{ipc}} \hat{H}_{\text{tot}} \rangle_T - \langle \hat{H}_{\text{ipc}} \rangle_T \langle \hat{H}_{\text{tot}} \rangle_T \right], \quad (\text{C9})$$

which still can be directly evaluated numerically within the NRG using complete basis sets.^{23,25,26} The term $\langle \hat{H}_{\text{ipc}} \rangle_T$ corresponds to a simple thermal average of a local quantity.²⁵ The total energy, on the other hand, is given by

$$\begin{aligned} \langle \hat{H}_{\text{tot}} \rangle_T &= \sum_{n,s \in D} \underbrace{\sum_e \frac{e^{-\beta E_s^n}}{Z}}_e (\omega_n \tilde{E}_s^n + \delta_n) \quad (\text{C10a}) \\ &= w_n(T) \frac{e^{-\beta E_s^n}}{Z_n} \equiv w_n \rho_s^n \end{aligned}$$

with the eigenenergies $E_s^n \equiv \omega_n \tilde{E}_s^n + \delta_n$ (as is customary, the NRG eigenenergies \tilde{E}_s^n are given in rescaled units,

with ω_n the energy scale at iteration n and δ_n here the *cumulative* subtracted energy offset w.r.t. the ground state at iteration n). While a global energy reference drops out of the entire definition of the impurity specific heat Eq. (C9), of course, the individual energy references δ_n for Wilson shell n *do not* cancel and hence must be properly included. Therefore $E_s^n \equiv \omega_n \tilde{E}_s^n + \delta_n$ represent the eigenenergies in non-rescaled physical units with respect to a single common energy reference, e.g. the ground state energy of the entire Wilson chain. In this case, the offsets δ_n , when computed starting from the low-energy side (i.e. large n) scale like $\delta_n \propto \omega_n$. In Eq. (C10a), finally, again a single sum over the complete discarded (D) basis set $(s, e, n)^D$ suffices, since, obviously, \hat{H}_{tot} commutes with itself, i.e. with the Hamiltonian used in the evaluation of the overall thermodynamic average. With the remaining term in Eq. (C9) given by,

$$\langle \hat{H}_{\text{ipc}} \hat{H}_{\text{tot}} \rangle_T = \sum_{n,s \in D} w_n \rho_s^n (\omega_n \tilde{E}_s^n + \delta_n) \langle s_n | \hat{H}_{\text{ipc}} | s_n \rangle, \quad (\text{C10b})$$

the resulting impurity specific heat can be expressed as follows,

$$\begin{aligned} c_V(T) &= \beta^2 \sum_{n,s \in D} w_n \omega_n \rho_s^n \tilde{E}_s^n \left[\langle s_n | \hat{H}_{\text{ipc}} | s_n \rangle - \langle \hat{H}_{\text{ipc}} \rangle_T \right] \\ &\quad + \beta^2 \sum_{n,s \in D} w_n \delta_n \rho_s^n \left[\langle s_n | \hat{H}_{\text{ipc}} | s_n \rangle - \langle \hat{H}_{\text{ipc}} \rangle_T \right] \\ &\equiv \sum_n w_n \left[\frac{1}{\omega_n} \tilde{c}_V^{(D,n)}(T) + \frac{\delta_n}{T^2} (\langle \hat{H}_{\text{ipc}} \rangle_n^D - \langle \hat{H}_{\text{ipc}} \rangle_T) \right], \end{aligned} \quad (\text{C11})$$

where $\tilde{c}_V^{(D,n)}(T)$ stands for the specific heat computed within the discarded states space of Wilson shell n in *rescaled* units, i.e. using \tilde{E}_s^n and $T \rightarrow \tilde{T}_n \equiv T/\omega_n$. While $\tilde{c}_V^{(D,n)}(T)$ is clearly independent of the energy references δ_n for each individual Wilson shell n , these δ_n do lead to a *finite* contribution through the very last term in Eq. (C11). The reason is that, in general, the thermal expectation value $\langle \hat{H}_{\text{ipc}} \rangle_n^D$ in the discarded state space of iteration n is unequal to the full thermal average $\langle \hat{H}_{\text{ipc}} \rangle_T$ for the entire system. Only for very late Wilson shells in the low energy fixed point, i.e. $T \rightarrow 0$, it follows $\langle s_n | \hat{H}_{\text{ipc}} | s_n' \rangle \simeq \langle \hat{H}_{\text{ipc}} \rangle_0 \cdot \delta_{ss'}$. This leads to cancellation of the last term, which is required for $\lim_{T \rightarrow 0} c_V(T) = 0$.

Appendix D: On the extraction of phase shifts within the NRG

The Kondo scale T_K^{FS} derived from the mixed susceptibility [see Eq. (4)] is identical to the Kondo scale T_K^φ obtained from the phase shifts [see Eq. (5)], i.e. $T_K^{\text{FS}} = T_K^\varphi$, as discussed with Eq. (6) in the main text. For a Fermi liquid in the thermodynamic limit, the one-particle level spacing can be considered equally spaced around the

Fermi energy yet different for each electronic flavor such as spin σ ,

$$\tilde{\epsilon}_{k\sigma} = \epsilon_{1\sigma} + k \cdot \epsilon_{2\sigma}, \quad (\text{D1})$$

with $k \in \{\dots, -2, -1, 0, 1, 2, \dots\}$ and $\epsilon_{1\sigma} \in [0, \epsilon_{2\sigma}[$, given that $\epsilon_{1\sigma}$ is essentially defined up to modulo $\epsilon_{2\sigma}$. Here the tilde on $\tilde{\epsilon}_{k\sigma}$ indicates that the original decoupled fixed bath modes may already have been shifted by the presence of a coupled impurity. If the baths are identical for each flavor σ including their discretization, $\epsilon_{2\sigma}$ is independent of σ . This is typically the case for NRG where $\epsilon_{2\sigma} \propto \omega_N \propto \Lambda^{-N/2}$, with ω_N the energy scale at large but finite length N of the Wilson chain. Hence $\epsilon_{1\sigma}/\omega_N$ and $\epsilon_{2\sigma}/\omega_N$ are both of order 1. For the ground state, all levels with $\tilde{\epsilon}_{k\sigma} < 0$ are occupied. If $\epsilon_{1\sigma} = 0$, the many-body ground state is degenerate. For a Fermi liquid, the phase shift φ_σ can be extracted independently for each σ . In the thermodynamic limit, it is given by the ratio

$$\frac{\varphi_\sigma}{\pi} = \frac{\epsilon_{1\sigma}}{\epsilon_{2\sigma}}, \quad (\text{D2})$$

(this can be simply motivated by using the connection of phase shifts to the change in (local) occupation through the Friedel sum rule, while taking a proper continuum limit starting from a finite yet large system, i.e. a discrete model).

Within the NRG, the one-particle level position in energy can be determined from the many-body eigenspectrum of the energy flow diagram, i.e. the finite-size fixed-point spectra at $T = 0^+$. This allows to extract φ_σ through Eq. (D2). Note, however, that due to the intrinsic even-odd alternations with the actual shell of the Wilson chain, the resulting phases φ_σ differ by the constant offset of $\pi/2$ between even and odd shells; nevertheless, since only differences in the phases due to the presence of the impurity, i.e. phase *shifts*, are considered, for an arbitrary but fixed energy shell this offset is irrelevant. However, Eq. (D2) is based on an equally spaced one-particle level spectrum around the Fermi energy, which is not quite the case within NRG at all! Even though NRG does allow to *directly* access the thermodynamic limit in the numerical simulation due to the underlying logarithmic discretization in Λ ,^{22,31} for a given length N of the Wilson chain and a necessarily rather coarse discretization with $\Lambda \gtrsim 2$, the approximately uniform level spacing around the Fermi energy quickly transforms into exponentially separated energy levels further away from the Fermi energy,³² as shown in Fig. 5.

Figure 5 analyzes the single-particle level spectra

for the interacting as well as the non-interacting SIAM [the latter also referred to as the resonant level model (RLM)] as defined in Eq. (9) for an arbitrary late but fixed even Wilson shell N [i.e. H_0 such as in Eq. (9) plus some larger even number of further Wilson sites; for an odd length of the Wilson chain, all curves in Fig. 5 would be trivially offset horizontally by $1/2$, which can be ignored]. With $\epsilon_d \equiv \{\epsilon_{d\sigma}\}$ the (magnetic field dependent) level positions of the impurity, the one-particle

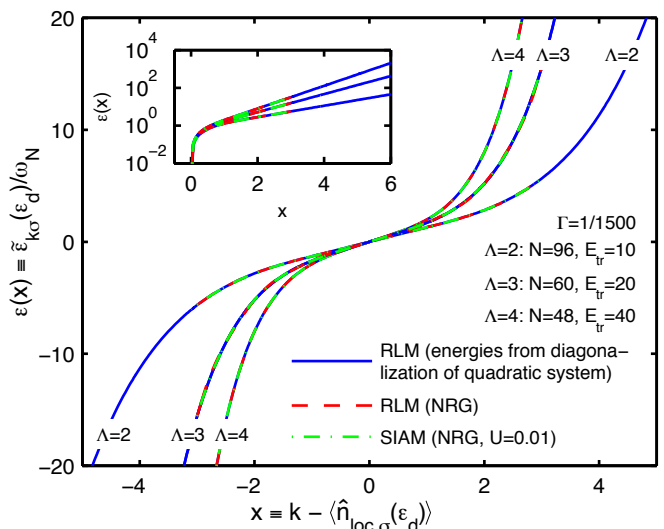


Figure 5. (Color online) Dependence of single-particle energy level spectra $\tilde{\epsilon}_{k\sigma}(\epsilon_d)$ on local occupation $\langle \hat{n}_{loc,\sigma}(\epsilon_d) \rangle$ and level index k for the SIAM [NRG (green dot-dashed)] as well as the RLM [quadratic solution (blue) and NRG (red dashed)] using a long even Wilson chain of length N as specified. The local occupation $\langle \hat{n}_{loc,\sigma}(\epsilon_d) \rangle$ and thus the phase shift is changed by varying the position of the impurity energy level $\epsilon_{d(\sigma)}$. While this level is swept from $+\infty$ to $-\infty$, $\langle \hat{n}_{loc,\sigma}(\epsilon_d) \rangle$ changes smoothly from 0 to 1. Combining all energies in units of the energy scale ω_n vs. $x \equiv k - \langle \hat{n}_{loc,\sigma}(\epsilon_d) \rangle$, this results in a single continuous antisymmetric curve $\epsilon(x)$ that is linear for small $|x|$, yet is quickly dominated by exponential behavior for larger $|x| \gtrsim 2$ (see inset and text). The discrete levels $\tilde{\epsilon}_{k\sigma}(\epsilon_d) < 0$ (i.e. within the range $x < 0$) correspond to single-particle levels below the Fermi energy and are thus occupied in the ground state. The data for the blue curve was obtained by numerical diagonalization of the quadratic Hamiltonian (RLM), hence all single-particle energies are easily obtained. In particular, their energies are not restricted to the energy range below the truncation energy, as is the case for the NRG-method (dashed and dot-dashed lines).

level spectrum $\tilde{\epsilon}_{k\sigma}(\epsilon_d)$ of the entire system. This shift of the discrete single-particle spectrum for an arbitrary but fixed ϵ_d is directly related to phase shifts via Friedel sum-rule. Thus when plotted vs. the *continuous* variable $x \equiv k - \langle \hat{n}_{loc,\sigma}(\epsilon_d) \rangle$ having $\epsilon_{d(\sigma)} \in [-\infty, \infty]$ and hence $\langle \hat{n}_{loc,\sigma}(\epsilon_d) \rangle \in [0, 1]$ with $\langle \hat{n}_{loc,\sigma}(\epsilon_d) \rangle$ the change in local charge at and close to the impurity¹⁸ depending on the impurity setting, this allows to collect all one-particle level spectra $\tilde{\epsilon}_{k\sigma}(\epsilon_d)$ after rescaling by the approximate one-particle level spacing ω_n into a *single continuous curve* $\epsilon(x)$, as demonstrated in Fig. 5. In a sense, with the Wilson chain in mind, the presence of the impurity allows to alter the boundary condition for the bath electrons, thus resulting in an impurity-dependent phase shift, which sets the horizontal offset $\langle \hat{n}_{loc,\sigma}(\epsilon_d) \rangle$ of the discrete energy levels in Fig. 5.

The resulting curve $\epsilon(x)$, which describes the *macroscopic* bath, is universal in the sense that it only depends on the bath discretization (i.e. Λ), but is independent of

the specifics of the *microscopic* impurity as long as the low-energy behavior represents an effective Fermi liquid. For example, as demonstrated in Fig. 5, the resulting curve $\varepsilon(x)$ is exactly the same independent of whether the impurity is interacting (SIAM) or not (RLM, with or without NRG). Using the same bath discretization for all flavors σ , as is customary within the NRG, this curve $\varepsilon(x)$ is also independent of σ , as already indicated by its notation.

As a consequence, for a given bath discretization the curve $\varepsilon(x)$ can simply be computed for the non-interacting case (spinless RLM) by repeated diagonalization of the underlying quadratic Hamiltonian while sweeping $\varepsilon_d \in [-\infty, \infty]$ (e.g. see solid line in Fig. 5). With the NRG bath-discretization being particle-hole symmetric, the resulting curve $\varepsilon(x)$ is antisymmetric in x , i.e. $\varepsilon(-x) = -\varepsilon(x)$. Then given the reference curve $\varepsilon(x)$ together with the requirement of its antisymmetry, the single-particle spectrum for any other impurity setting can be fitted (provided Fermi liquid behavior), which allows to extract the horizontal offset $\langle \hat{n}_{\text{loc},\sigma}(\varepsilon_d) \rangle$ and hence the phase shift φ_σ independently for each flavor σ , *even if* the single-particle spectrum is not exactly uniformly spaced around the Fermi energy.

The range of linearity of $\varepsilon(x)$ around $x = 0$ indicates the regime of equally spaced single-particle levels closest to the Fermi energy, given an exponentially large but fi-

nite system size, as represented by the length N of the Wilson chain. For $\Lambda = 2$, linearity is given to a good approximation (within about 0.8%) for $x \in [-0.5, 0.5]$, i.e. for the lowest single-particle and single-hole excitation in the particle-hole symmetric case, and hence justifies using Eq. (D2) [this method was used for extracting T_K^φ and verifying Eq. (6) to within 1% accuracy in the main text]. In contrast, for $\Lambda = 4$ the linearity of $\varepsilon(x)$ even within this minimal regime is already clearly compromised (about 3%). Here usage of Eq. (D2) already leads to clear systematic errors due to the strongly increased coarseness of the underlying logarithmic discretization, leading to about a 7% error in Eq. (6). Therefore the extraction of phase shifts for larger Λ from the single-particle spectra requires a more careful analysis such as the aforementioned fitting to the curve $\varepsilon(x)$. Given logarithmic discretization, it follows that $\varepsilon_k \sim \text{sgn}(k) \omega_N \Lambda^{|k|}$ for larger $|k|$ for a fixed length N of the Wilson chain. From the semilog-y representation in the inset of Fig. 5 it can be seen, that for $|x| \gtrsim 2$, $\varepsilon(x)$ is already described by a plain exponential behavior to within 0.1%. Thus rather than fitting the data for $|x| \lesssim 1$, alternatively, one may simply concentrate on the exponential behavior for larger $|x|$ which, however, requires to extract the single particle spectrum at least up to the third single particle level.

-
- ¹ J. Kondo, Progress of Theoretical Physics **32**, 37 (1964).
² C. Bäuerle, F. Mallet, F. Schopfer, D. Maily, G. Eska, and L. Saminadayar, Phys. Rev. Lett. **95**, 266805 (pages 4) (2005).
³ F. Mallet, J. Ericsson, D. Maily, S. Ünlübayir, D. Reuter, A. Melnikov, A. D. Wieck, T. Micklitz, A. Rosch, T. A. Costi, et al., Phys. Rev. Lett. **97**, 226804 (pages 4) (2006).
⁴ T. A. Costi, L. Bergqvist, A. Weichselbaum, J. von Delft, T. Micklitz, A. Rosch, P. Mavropoulos, P. H. Dederichs, F. Mallet, L. Saminadayar, et al., Phys. Rev. Lett. **102**, 056802 (2009).
⁵ D. Goldhaber-Gordon, H. Shtrikman, D. Mahalu, D. Abusch-Magder, U. Meirav, and M. A. Kastner, Nature **391**, 156 (1998).
⁶ A. V. Kretinin, H. Shtrikman, D. Goldhaber-Gordon, M. Hanl, A. Weichselbaum, J. von Delft, T. Costi, and D. Mahalu, Phys. Rev. B **84**, 245316 (2011).
⁷ P. Nozières, J. of Low Temp. Phys. **17**, 31 (1974).
⁸ M. Grobis, I. G. Rau, R. M. Potok, H. Shtrikman, and D. Goldhaber-Gordon, Phys. Rev. Lett. **100**, 246601 (2008).
⁹ M. Pletyukhov and H. Schoeller, Phys. Rev. Lett. **108**, 260601 (2012).
¹⁰ L. Merker, S. Kirchner, E. Muñoz, and T. A. Costi, Phys. Rev. B **87**, 165132 (2013).
¹¹ M. Hanl, A. Weichselbaum, T. A. Costi, F. Mallet, L. Saminadayar, C. Bäuerle, and J. von Delft, Phys. Rev. B **88**, 075146 (2013).
¹² A. Hewson, *The Kondo Problem to Heavy Fermions* (Cambridge University Press, New York, 1993).
¹³ T. A. Costi, Phys. Rev. Lett. **85**, 1504 (2000).
¹⁴ R. Bulla, T. Costi, and T. Pruschke, Rev. Mod. Phys. **80**, 395 (2008).
¹⁵ A. Dirks, S. Schmitt, J. E. Han, F. Anders, P. Werner, and T. Pruschke, EPL (Europhysics Letters) **102**, 37011 (2013).
¹⁶ M. Höck and J. Schnack, Phys. Rev. B **87**, 184408 (2013).
¹⁷ B. S. Shastry, E. Perepelitsky, and A. C. Hewson, arXiv:1307.3492 [cond-mat.str-el] (2013).
¹⁸ W. Münden, A. Weichselbaum, M. Goldstein, Y. Gefen, and J. von Delft, Phys. Rev. B **85**, 235104 (2012).
¹⁹ M. Le Bellac, F. Mortessagne, and G. G. Batrouni, *Equilibrium and Non-Equilibrium Statistical Thermodynamics* (Cambridge University Press, Cambridge, 2004), ISBN 0-521-82143-6.
²⁰ J. Friedel, Advances in Physics **3**, 446 (1954).
²¹ P. W. Anderson, Phys. Rev. Lett. **18**, 1049 (1967).
²² K. G. Wilson, Rev. Mod. Phys. **47**, 773 (1975).
²³ A. Weichselbaum and J. von Delft, Phys. Rev. Lett. **99**, 076402 (pages 4) (2007).
²⁴ A. Weichselbaum, Annals of Physics **327**, 2972 (2012).
²⁵ A. Weichselbaum, Phys. Rev. B **86**, 245124 (2012).
²⁶ F. B. Anders and A. Schiller, Phys. Rev. Lett. **95**, 196801 (2005).
²⁷ L. N. Oliveira, V. L. Libero, H. O. Frota, and M. Yoshida, Physica B: Condensed Matter **171**, 61 (1991), ISSN 0921-4526.
²⁸ W. Hofstetter and S. Kehrein, Phys. Rev. B **59**, R12732 (1999).
²⁹ L. Merker and T. A. Costi, Phys. Rev. B **86**, 075150 (2012).

- ³⁰ L. Merker, A. Weichselbaum, and T. A. Costi, Phys. Rev. B **86**, 075153 (2012).
- ³¹ A. Weichselbaum, W. Munder, and J. von Delft, Phys. Rev. B **84**, 075137 (2011).
- ³² H. R. Krishna-murthy, J. W. Wilkins, and K. G. Wilson, Phys. Rev. B **21**, 1003 (1980).